2-D Material Sensors on the Electronic Nose for the Sensitive Detection of VOC

Thesis by

Kyra SoHyun Lee

In Partial Fulfillment of the Requirements for

the degree of

Chemistry

CALIFORNIA INSTITUTE OF TECHNOLOGY

Pasadena, California

2020

Defended June 4, 2020

Kyra SoHyun Lee

ORCID: 0000-0002-2100-1534

ACKNOWLEDGEMENTS

This work has been an incredible part of my journey. I would like to thank my families, friends, Nate Lewis and the Lewis Group for supporting me and being by my side throughout this process. I am eternally grateful to everyone for supporting me as I grew, not only personally, but also through my research.

I would like to personally thank Nate, Barbara and Kimberly, Ellen, Annelise, and Sean from the Lewis Group for all the research and incredible moral support they have given me to help me to grow.

ABSTRACTS

Chapter 1

When coated with a polymer surface layer and suspended on 3-D textured glass electrodes, the hybrid combination of polymer and graphene yields sensitive chemiresistive vapor sensors. The expansion and contraction of the polymer layer when it absorbs/reacts with the VOCs, is proposed to produce tremendous train on the suspended graphene. Hence, when VOCs permeates into the polymer layer, sizable electrical resistive changes as folds and creases is induced in the graphene due to its high gauge factor. The hybrid suspended polymer/Gr sensor exhibits substantial responses to polar organic vapors, especially pyridine, while also exhibiting reversibility and the potential future tunability in the types of polymers used as the reactive surface layer.

Chapter 2

Various polar and non-polar functional groups were covalently bonded onto MoS_2 yielding incredibly sensitive chemiresistive vapor sensors. The VOCs' interaction to the functional end groups produced tremendous signal, while also exhibiting reproducibility and reversibility. Future work will further standardize the sensors while also exploring tunability in the types of groups used.

Chapter 3

This chapter reflects the very start of my PhD research, and one of the important lessons to learn about the electronic nose. It is an example that I wish my predecessors taught me (all had graduated by the time I began my research) that I hope to pass onto

future nose users. It is just one example of many projects that had similar end result. Many key lessons can be learned for future nose users. Readers can choose to skip reading this.

PUBLISHED CONTENT AND CONTRIBUTIONS

Lee, S. et al. (2020). “Strain-based chemiresistive polymer-coated graphene vapor sensors”. In: Materials Nanoletters. Submitted Aug 2020.

- Lee, S. participated in conception of the project, solving, analyzing, prepared the data and participated in writing the manuscript.

TABLE OF CONTENTS

C h a p t e r 1

GRAPHENE STRAIN SENSORS ON TEXTURED ELECTRODES

Lee, S. et al. (2020). “Strain-based chemiresistive polymer-coated graphene vapor sensors”. In: Materials Nanoletters. Submitted May 2020

Introduction

Artificial olfactory systems, or electronic noses, has for a number of years attracted great interest for a number of applications such as air quality checking, disease diagnostics, and etc. Based on an array of cross-reactive, chemically sensitive resistive sensors provide a simple technological implementation of a vapor detection by mimicking the functionality of biological olfactory systems. When exposed to volatile organic vapors, the analyte chemi-adsorbs and/or reacts with the sensing material of interest, thereby producing a change in resistance. The various volatile organic compounds (VOCs) of interest are recognized and classified using pattern recognition algorithms and a neural network. [9,10,11] Previous electronic nose sensors were developed using a variety of materials such as intrinsically conducting or non-conducting polymers loaded with conducting material such as carbon black and graphene, as well as individually functionalized metallic nanoparticles and other related systems.[9, 11]

Two-dimensional materials such as graphene have shown boundless potential for sensors as well as in numerous different applications such as nano-electronics, and biomedical technologies, while also providing adaptable and flexible architectures to further

its potential and use.[13,18,19,21] Monolayer graphene is exclusively composed of sp^2-hybridized carbon atoms equipped with free p_z orbitals where the p_z-orbitals are responsible for the incredible electronic sensitivity of graphene, leading to its incorporation of graphene in various electrical, and chemical sensors. Hybrid material sensors of a combination of graphene and various other materials such as nanoparticles and/or polymers have also been widely explored.[12]

Overlaying graphene across columns or over channels to suspend it, yields an approach to creating a very sensitive strain-based graphene sensor producing large effects on the nano-molecular scale. Large chemiresistive responses were previously observed when an overlay of monolayer graphene on one-dimensional (1D) ZnO rods was exposed to polar analytes.[13] Previous exploration on suspension of graphene monolayers were fabricated using time-intensive methods such as electron-beam lithography complicating its mass scale up with its sensitive architecture.

Particularly graphene pressure sensors are known in literature to be extremely sensitive to small changes when stimulated where strain can be translated into large signals. These strain-based graphene devices when subjected to large compressive or inflation forces, results in a flexible deformation of the graphene lattice, producing large variations in the resistance of graphene at the surface. Herein, our specific strain sensor was developed by layering a monolayer graphene in a stretchable polymer where-in this strain-based approach is possible because the graphene lattice can undergo significant amounts of deformation without shattering.[1] Typically, usage of hybrid polymer-coated graphene monolayers are less frequently employed as a chemi-resistive sensors due to graphene's chemical inertness and the typical polymer integrated with graphene (i.e. polydimethysiloxane PDMS) does not

respond well to various VOCs.[20] However, strain-based sensors often have extremely high gauge factors, providing quantifiable changes in resistance with minute amounts of deformation.[2,7] Also, utilizing various polymers along with the graphene produces hybrid synergistic effects while also substantially improving the robustness of the graphene.

Sensors integrated with just singular layer of graphene alone deteriorates from a lack of sensitivity, due to monolayer graphene's natural chemical inertness. Therefore, limited covalent functionalization has become a pervasive method to control the physical, optical, and electrical properties of graphene. However, across graphene's basal plane the uneven distribution of functional groups poses a hurdle to the integration of covalently functionalized graphene into commercially scalable devices due to the typical requirement of the high degree of fidelity necessary for a successful scale-up. Current methods for covalent functionalization often use the defects in graphene's basal plane to attach various functional groups to its surface-however this method decomposes the quality of the graphene lattice.[14] Therefore, graphene polymer hybrid material composites have been introduces to explore new functionalities without compromising its structure/basal plane. Hybrid polymer composites offer greater reproducibility and strength than either the polymer or graphene alone. [18] However, these composites although have been used in several device implementations, they still require the usage of oxidized graphene flakes instead of pristine graphene.[16,17,18]

Herein we describe the facile fabrication method for the suspended hybrid monolayer graphene producing a chemi-resistive sensor with incredible responsivity to pyridine and various other VOCs. A textured 3-D pillar silicon oxide electrode substrate was developed to suspend and support the hybrid graphene substrate. By hanging or suspending the

graphene on these columns/textured electrodes, the hybrid material is given the ability to enlarge and move in the x-y-z plane because of the polymer overlayer reacting to the various VOCs. Therefore, as the suspended material expands and contracts, we can exploit the chemical and physical properties of the graphene as various curvature, folds and creases is induced within the material, changing its electronic properties. Numerous studies have reported the properties that result from folding and wrinkling of graphene, as well as the unique behavior due to the curvature of suspended graphene under mechanical stimulation.[13] As a result, the resulting chemiresistive sensors can access both the sensitivity of the graphene monolayer and the specific response to organic vapors of different polymer overlayers.

Methods

Materials

CVD-grown monolayer graphene on Cu (Cu/Gr) was purchased from Advanced Chemical Supplier Materials with grain sizes reported by the manufacturer to be 50 μm in diameter. Poly (ethylene-*co*-vinyl acetate) (PEVA: vinyl acetate at 18 weight %) was purchased from Sigma Aldrich while black pearls 2000 carbon black (CB) was purchased from Cabot Corporation. All solvents were obtained from VWR and Sigma Aldrich and used without further purification.

Sensor Fabrication

All methods for textured 3-D pillar sensor electrode preparation was conducted in a class 100 cleanroom, where the initial SiO_2 (Glass) slides obtained from VWR first undergoing

cleaning using acetone and isopropanol. After it was baked in the oven at 170 °C and cooled to room temperature. Microposit S1813 photoresist (MicroChem) was placed on the slide (covering the whole slide) and spun at 500 rpm for 30s followed by 4000 rpm for 60s where it was finally proceeded by a 10 s exposure to a mask using a 425 nm lamp in a contact mask aligner (Suss MicroTech MA6/BA6). The photoresist covered glass slide was placed in MF-319 developer (MicroChem) for 90 s for development. After lift-off, the slide was washed with water and placed in the e-beam evaporator where columns of different heights were grown on the patterned slide by deposition of 50 to 300 nm of SiO_2 (CHA Industries Mark 40). Lift-off was finalized using remover PG (MicroChem) for 45 min sonicating at 60 °C. Electrode contacts on the pillar electrodes were formed by evaporating 5-10nm of Ti, followed by 50-70 nm of Au where the 2 metallic electrode were separated by a 0.1 cm. 4% PEVA solutions were made by placing respectively weighted PEVA into toluene where it was sonicated for 4hrs until the PEVA was well-dispersed. To create the polymer hybrid graphene sensors, monolayer of graphene (Cu/Gr) grown on top of a layer of Cu was purchased from graphene supermarket and was coated with a layer of PEVA at various specified rpm rate (varied from 1000-8000rpm depending on thickness) for 60s, where it was cured for 1min at 150 °C. The Cu sheet was cut into smaller pieces, usually around ~1cm x 3 mm (active area ~0.1-0.2 cm^2) where it was etched using $FeCl_3$ solution (Copper etch, Transene) until Cu dissolved (~1.5hrs). The Gr/PEVA piece was than transferred to a water bath ($\geq$18.2 MΩ-cm resistivity H_2O) and after 1 h it was transferred to a second clean H_2O bath, in which the sample was left for 12-24 h. After the 2nd bath, the material was transferred to a final fresh H_2O bath, where the material was placed onto the 3-D pillar substrate/electrode and dried using a N_2(g).

The controls were fabricated with similar techniques with variations of column height (50 to 300 nm of SiO_2, and variation of polymer thickness: 1000-8000rpm as stated above). Solutions of 4% by weight PEVA and 1 wt. % CB were sonicated by sonicating the respective amount of PEVA needed with toluene first for 4hrs followed by 1 wt.% CB for 2hrs. The PEVA/CB solution was then spun onto a Cu substrate and transferred to respective electrodes of interest by etching away the copper followed by a wash with water as described above. Gr without a PEVA coating was transferred with a supporting layer PMMA where it was spun at 3000 rpm for 60 s. Gr/PMMA was transferred to an electrode and washed with acetone for 10min after transfer onto the electrode of interest.

Sensor Measurements

Sensors were tested using a setup previously described on respective electronic noses of the Lewis Group.[9,10,11] Organic vapors were generated by N_2(g) flow background delivery at a flow rate of 3000 mL min^{-1} through 45 cm bubblers that had been filled with the suitable VOC solvents.[9] Volumetric ratio mixing allowed for analyte concentration to be measured and adjusted where the analyte stream was mixed and flowed using background N_2(g) stream controlled by mass flow controllers. Before the start of each experiment run, 700s of background gas was run which was proceeded by respective analyte exposure. Each analyte exposure comprised of 200 s of N_2 background gas, followed by 80 s of analyte (VOC) gas, and then 200 s of background gas at a flow rate of 3000 ml min^{-1}. The sensors were clipped into a long rectangular, 16 electrode chamber which was connected to the gas delivery system using chemical resistant tubing. The resistance measurements from each sensors was measured by a Keysight technologies 34970A data acquisition/switch unit with a Keysight

34903A 20 Channel Actuator. Data was collected via a GPIB connection to a computer where the experimental programming was controlled using LabVIEW software.

Differentiation ability of the Gr/PEVA column sensors was envisioned using Principal component analysis (PCA) and a neural network. PCA was performed on 16 individual hybrid graphene polymer arrays where for all the VOCs, 20 randomized test exposures of various VOCs of interest were recorded at $P/P^o = 0.0050$ at room temperature.

Sensor Characterization

Profilometry data of the polymer thickness used in the controls were obtained on a Bruker Dektak XT profilometer equipped with a 2 μm tip radius probe.

Signal Processing

All data processing was using custom formulations in Origin and R. The $\Delta R_{max}/R_b$, was calculated from R_{max},, the baseline-corrected maximum response upon exposure to the VOC of interest, vs. the baseline resistance under inert N_2 before exposure. S_R values were calculated using linear least-squares fitting of the steady-state change in frequency vs. analyte concentration.

Sensor discriminant performance was visualized using principal component analysis (PCA). The normalized data were mean-centered, and the diagonalized data set of the covariance matrix was transformed into sets of dimensions in terms of principal components (PCs), where the largest amount of variance is taken in the 1st PC while the 2nd PC captured the second most variance while being orthogonal to the first PC. The normalized mean-centered data were projected onto the 1st and 2nd PCs as shown in figure 7, in accord with

their respective coordinate vectors as observed through their corresponding eigenvalues and eigenvectors.

Results/Discussion

The response from the sensors was measured as the change in resistance (ΔR_{max}) over the baseline resistance (R_b), where R_p was the point taken just before respective VOC delivery was halted.

$$S = \frac{R_p - R_b}{R_b} * 100 = \frac{\Delta R}{R_b} * 100 \quad (1)$$

Control sensors were fabricated to compare their responses to those of the optimized sensor design. Polymer composite sensors usually comprises of a mixture of a conductive material such as CB and an insulating polymer. The amount or the percent composition by weight of CB is determined by the optimal baseline resistance of the chemoreceptive sensor device and optimal sensitivity. The sensors here utilizes a conductive monolayer of graphene as its conductive material. The control samples included graphene alone on a flat interdigitated electrode; graphene on 150 nm columns; and PEVA/CB transferred or sprayed onto flat interdigitated substrates as well as 150nm 3-D columns (Figure 1). Strikingly, the PEVA/CB composite sprayed onto the surface of a substrate showed a large negative response to ethanol and ethyl acetate, in accord with behavior that has been reported previously for such sensors, whereas the PEVA/CB composites formed as uniform films showed a positive response to these analytes[5] (Figure S1). The PEVA/CB composites used herein were developed using 4% PEVA films as compared to 2% PEVA/CB films deposited by an air brush because 4% PEVA was the lowest concentration that was secure enough to allow for graphene transfer.

For the majority of the analytes, PEVA/GR (col) exhibited the largest sensitivity, with the exception of toluene and ethanol. For both toluene and ethanol, PEVA/CB (col) showed the largest sensitivity. Figure 2 shows the overlay of responses of the sensor coated with Gr/PEVA to a single pulse of various concentrations of pyridine vapor. Upon exposure of the sensor to the analyte, the resistance steadily increased until the analyte was purged from the chamber, at which point the resistance decreased very slowly and flattened. The pulse peaks for the Gr/PEVA (col) were slower to respond and slower to recover whereas the other controls (graphene alone (Col), 4% PEVA/CB (col), 4% PEVA/CB (Flat)) exhibited much smaller but more rapid, and more reversible peaks (S1, S2, S3, S4). 4% PEVA/CB on flat and column controls was more reversible than plain graphene on columns after analyte exposure. This behavior suggests that the PEVA polymer overlayer with graphene makes the sensor less flexible and perhaps stiffer and slower in its recovery, but exhibits higher resistance change when strained. The other controls (graphene alone (flat), 4% PEVA/Gr (Flat) produced lower and/or more noisy sensor responses.

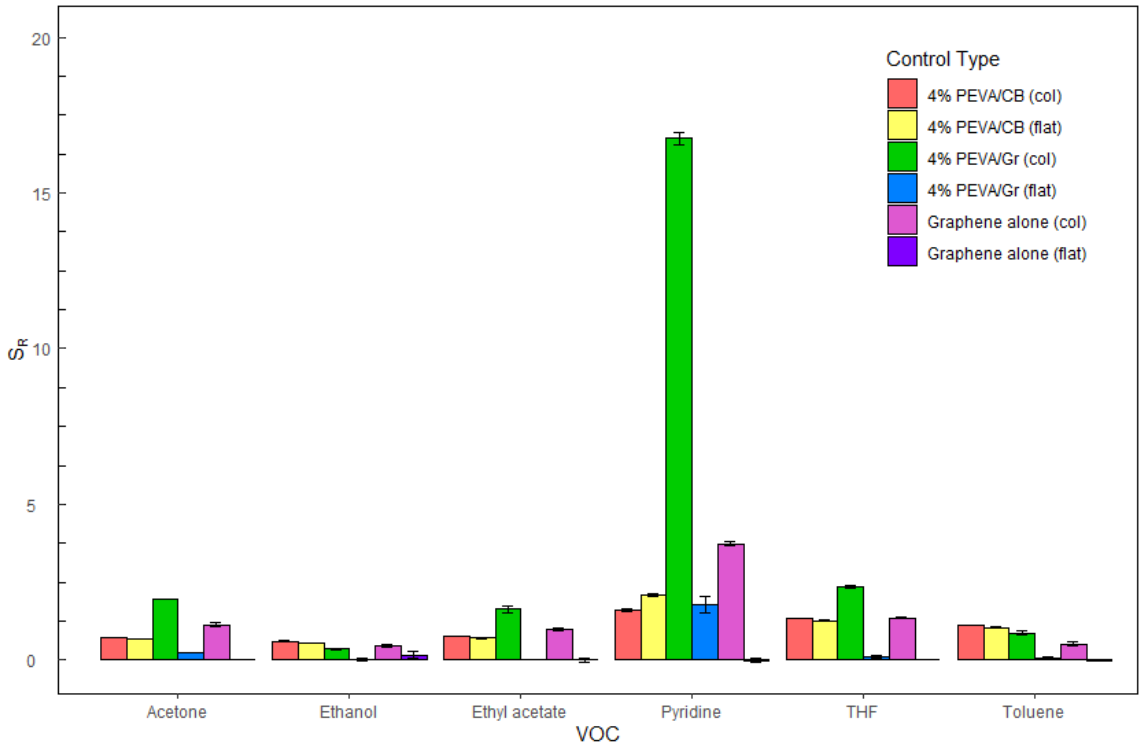

Figure 1. S_R values for the control sensors versus PEVA/Gr on columns exposed to various VOC partial pressures as a fraction of the analyte vapor pressure (P/P^o) at a flow rate of 3000 ml min^{-1} under N_2 as the carrier gas. The S_R value was the highest for 4% PEVA/Gr (col) for majority of the analytes. This geometry produced larger relative differential

resistance changes than analogous PEVA/-CB or graphene chemiresistive sensors, under nominally similar test conditions.

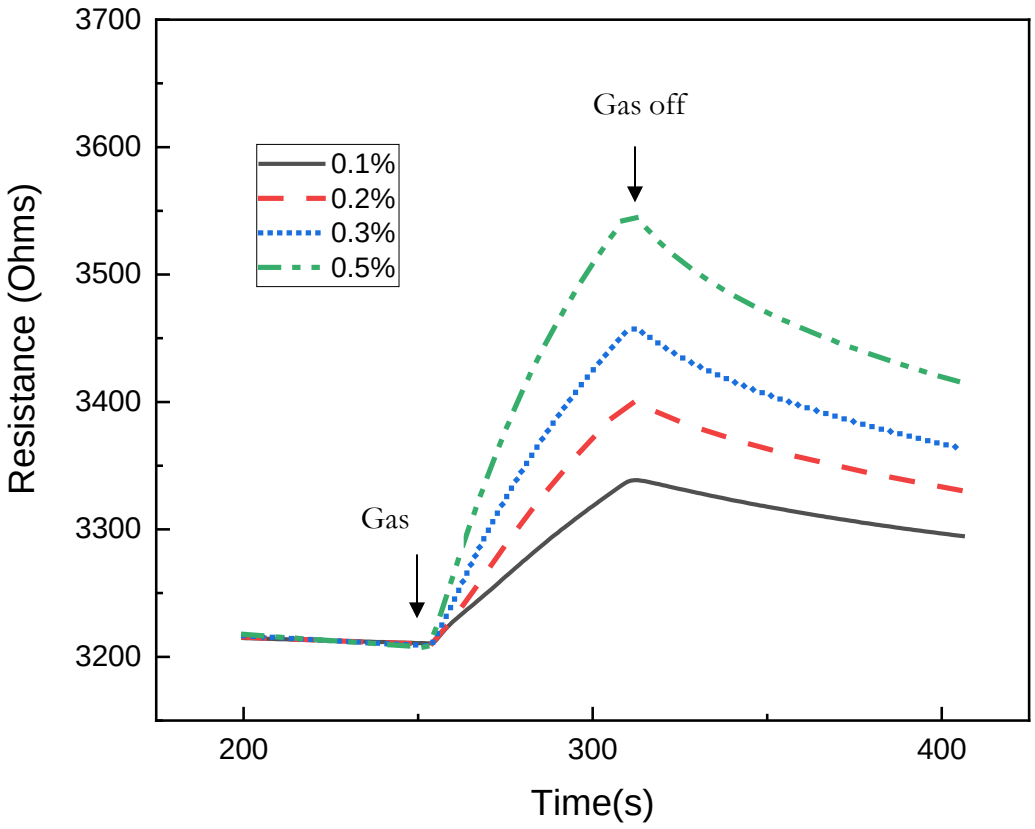

Figure 2. Typical sensor responses when exposed to P/P^o=0.0010, 0.0020, 0.0030, 0.0050 of pyridine at a flow rate of 3000 ml min^{-1} under N_2 as the carrier gas. The times at which the sensor was exposed to the analyte and purged with the carrier gas, respectively, are marked on the plot.

The column height was varied to ascertain the optimal response of the sensors. For most analytes, a 150 nm pillar height exhibited the highest sensitivity, except pyridine and toluene, for which the sensitivity increased substantially as the column height increased.

Pyridine and toluene are similar in chemical structure both equipped with aromatic rings, suggesting that greater column height allows for more area for the sensor to expand/contract possibly due to similar strain prompted by exposure to pyridine or toluene.

The thickness of the polymer overlayer was varied to obtain the optimal response for the sensors to the VOCs evaluated in this work (Figure 4). Figure 4 shows the responses for sensors with the polymer overlayer deposited at speeds between 1000 and 8000 rpm. 75 nm (6k) thick films showed the largest sensitivity to most analytes except for toluene, with the responses decreasing substantially for sensors having thinner layers of PEVA.

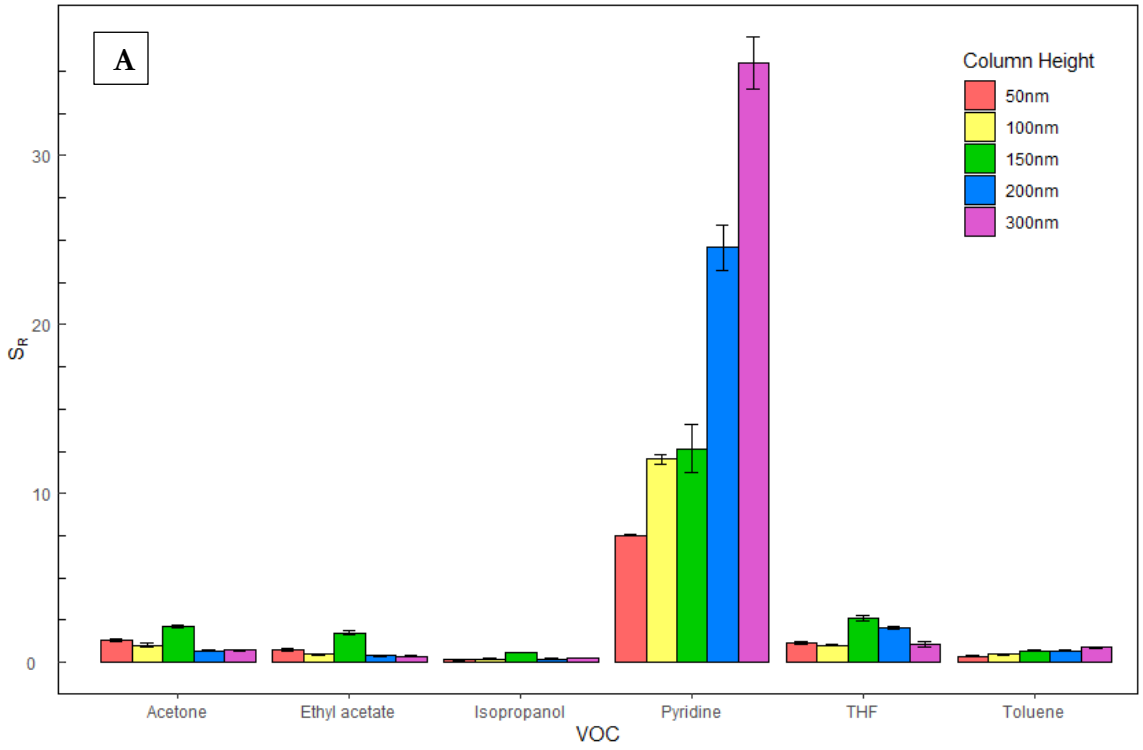

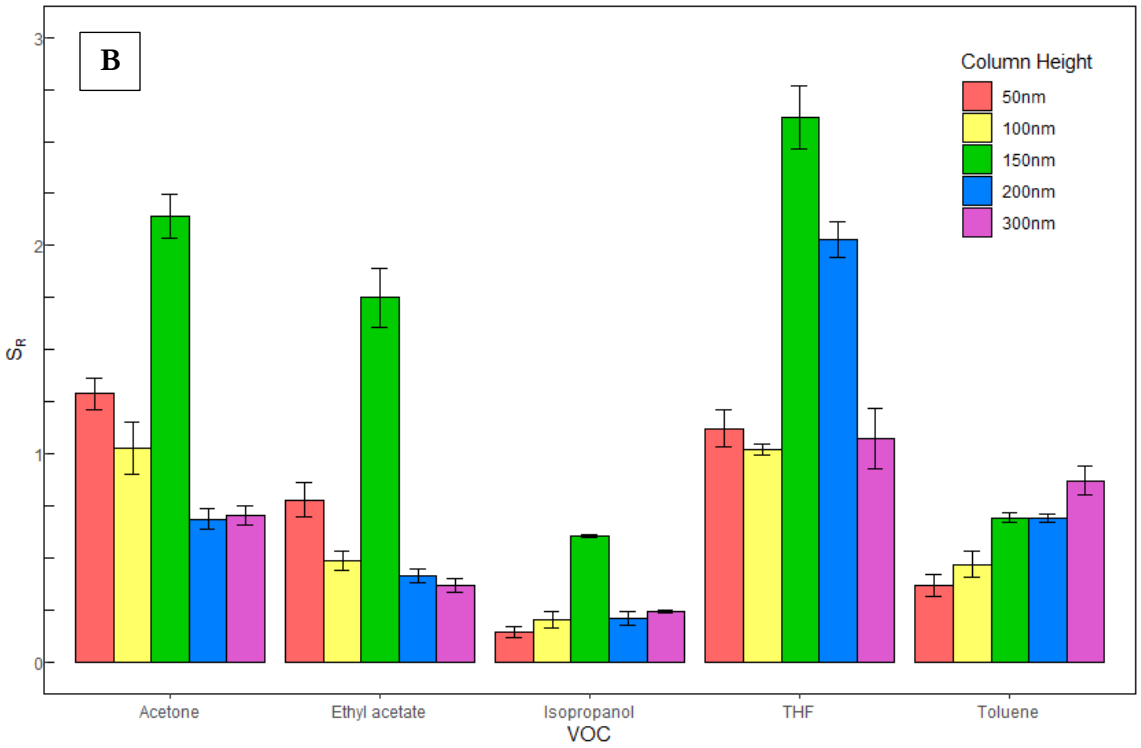

Figure 3. A) S_R values for controls of column pillar height for suspended hybrid grapheme sensors exposed to various VOC partial pressures as a fraction of the analyte vapor pressure (P/P^o) at a flow rate of 3000 ml min^{-1} under N_2 as the carrier gas. Pyridine characteristically exhibited an increase in response as column height increased. B) An expanded ordinate of the responses except for pyridine. For the majority of VOCs, 150 nm column heights produced the largest response.

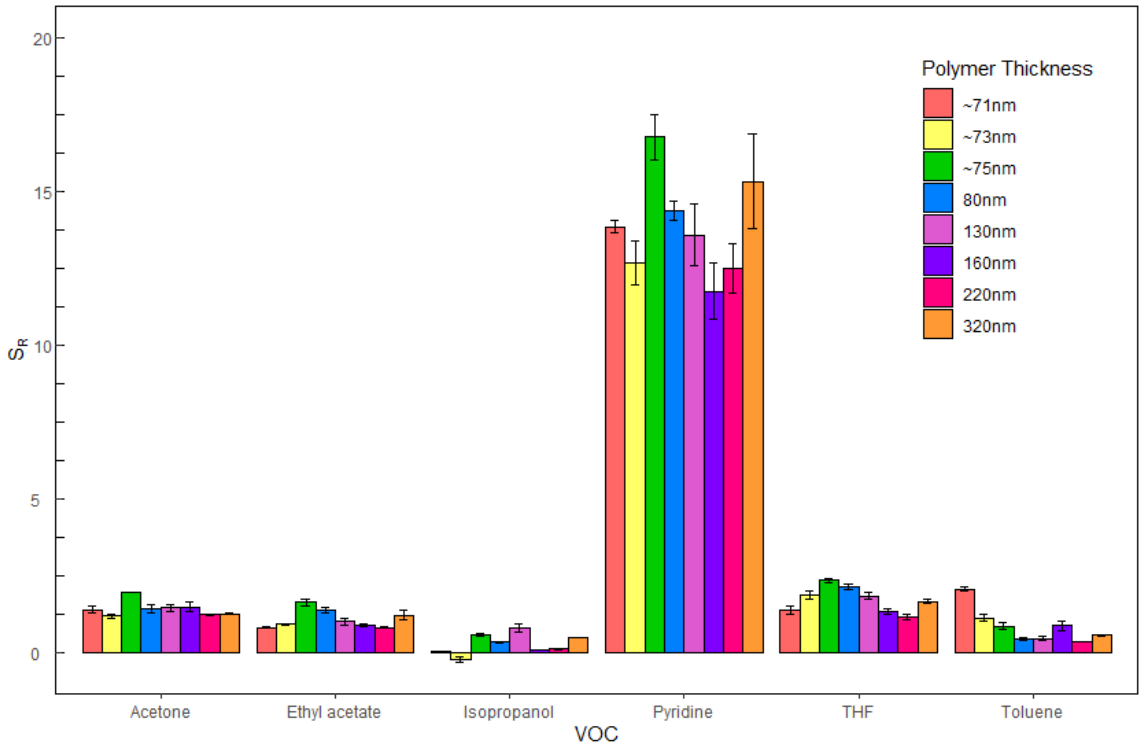

Figure 4. S_R values of controls for polymer overlayer thickness exposed to various VOC partial pressures as a fraction of the analyte vapor pressure (P/P_o) at a flow rate of 3000ml min^{-1} under N_2 as the carrier gas. The quoted spin speed in rpm produced a polymer film of thickness: 1k (320 nm), 2k (220 nm), 3k (160 nm), 4k (130 nm), 5k (80 nm), 6k (~75 nm), 7k (~73 nm), and 8k (~71 nm), respectively. A spin speed of 6k (~75 nm resulting film thickness) produced the best response for majority of the exposures. S_R values were larger for pyridine than the other VOCs tested.

The sensors were similarly optimized for the number of columns on the substrate (Figure 5). The standard pattern had columns with 3 μm diameter and a pitch of 7 μm. The pitch was then varied between 7 and 120 μm, with a constant thickness of polymer overlayer and size of the transferred Gr/PEVA sheet. The sensor response decreased as the number of

columns decreased (S5). Figure 5 shows that the response exhibited a plateau at ~5x10^5 columns.

Reproduciblity was tested through constant, repeated, mulitple measurements of a VOC of interest. In Figure 6a the optimized sensor was exposured to x100 pyridine at P/P^o = 0.0010, where P is the pressure of the analyte and P^o is the vapor pressure of the analyte at room temperature. The response decreased over time as it was exposed to repeated expsorues of pyridine as shown in figure 6b (P/P^o = 0.0030 acetone under nitrogen carrier gas at 3000 ml min^{-1}) (Figure 6b). However when the sensor was allowed to recover under N_2(g)for an extended period of time (24hrs), the sensor recovered the full response before such exposure.

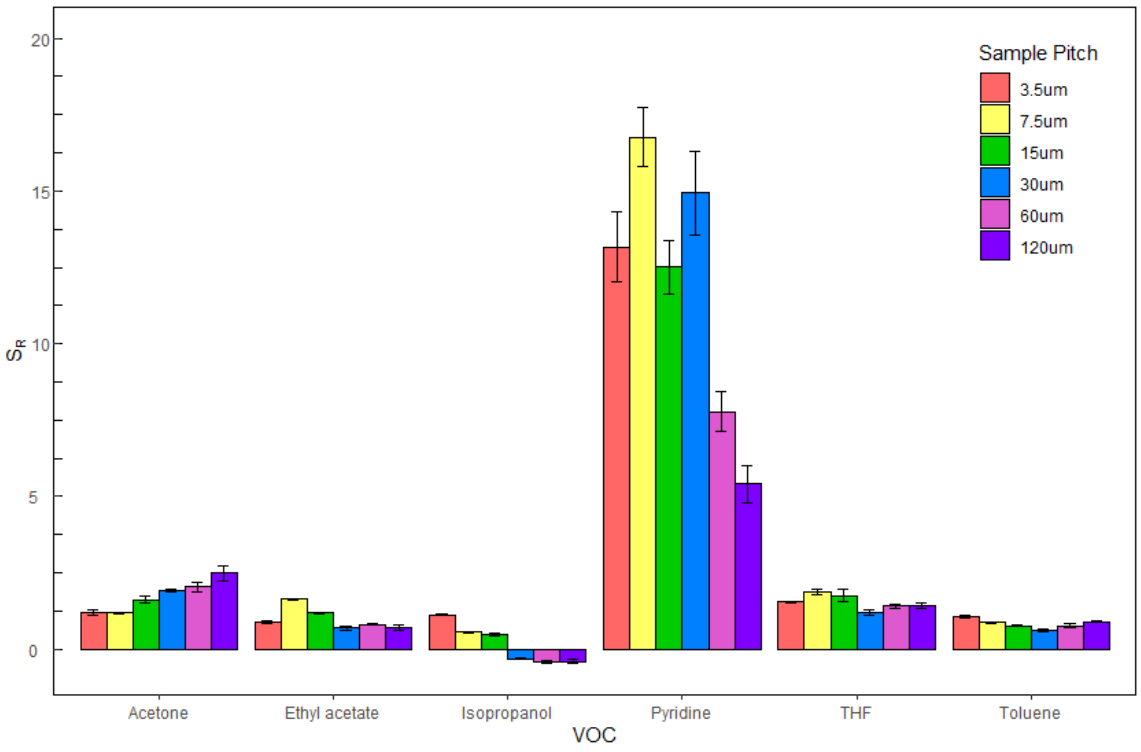

Figure 5. S_R values of controls for columns/pitch of the substrate at various VOC partial pressures as a fraction of the analyte vapor pressure (P/P_o) at a flow rate of 3000 ml min^{-1}

under N_2 as the carrier gas. The number of columns correlated to the pitch as 4.3 million columns (3.5 µm), 2 mil (7.5 µm), 1 mil (15 µm), 500 k (30 µm), 250 k (60 µm), and 125 k (120 µm), respectively. S_R values were largest at 7.5 µm pitch for ethyl acetate, pyridine, and THF.

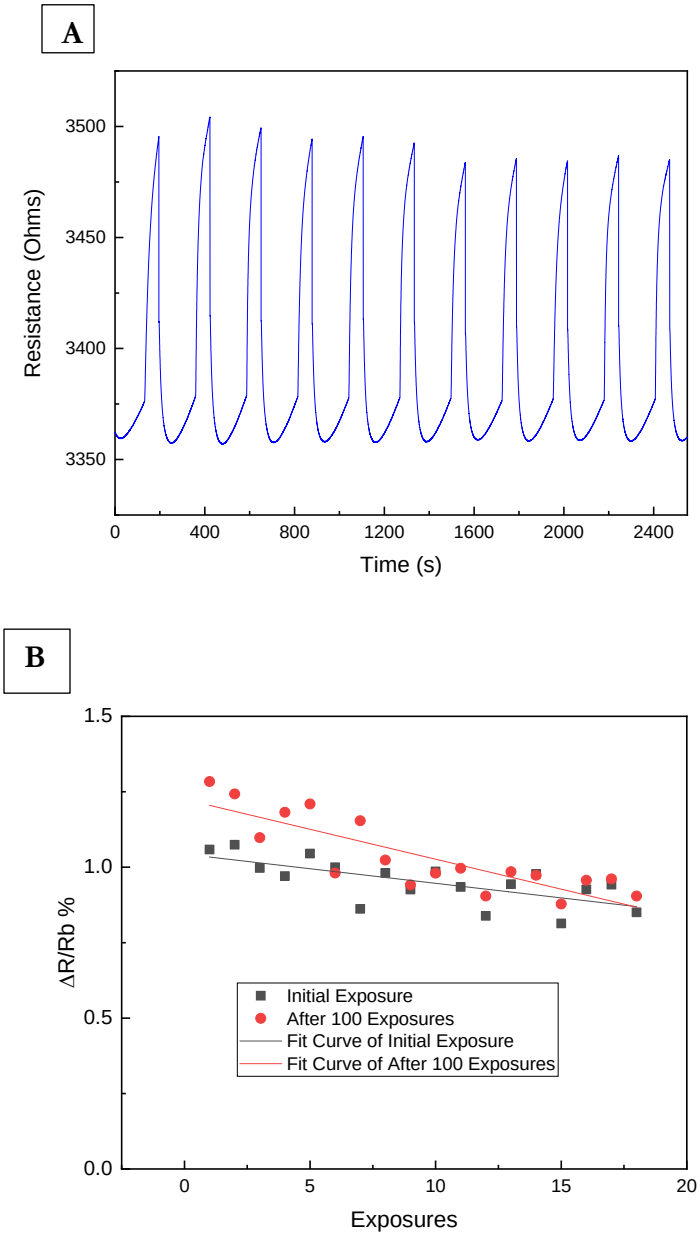

Figure 6. A). Optimized pyridine response at $P/P^o = 0.0010$ (nitrogen carrier gas at a flow rate of 3000 ml min^{-1}) showing reproducability with repeated exposure with 200 s under N_2 between exposures. B) Comparison of initial 20 exposures (black) vs sensor response after being exposed to 100 pyridine exposures at $P/P^o = 0.0010$ (red) under N_2 as the carrier gas at a flow rate of 3000 ml min^{-1} after being allowed to recover for 24 h under N_2(g).

Discrimination performance was analyzed using PCA (Figure 8). The 1st and 2nd projections of the PCs shows that the hybrid graphene polymer sensor array clearly separated polar from non-polar vapors. Although overlaps between data clusters were observed especially for some of the aprotic polar vapors (THF, ethyl acetate, and acetone), the responses of aprotic and protic polar vapors (Isopropanol, ethanol) were mutually discriminated. Moreover, pyridine generally exhibited the highest resistive response and produced a unique fingerprint relative to its aprotic polar counterparts. DMF also exhibited a clear separation from other VOC's, similar to pyridine. This behavior suggests that the amine/amide group has a specific electronic/strain effect on the graphene/polymer hybrid arrays.

Unmodified graphene has been used previously as a chemical sensor. Similar to the hybrid graphene/polymer sensor, an increase in resistance was observed for ethers (THF) and ketones (acetone), whereas a decrease in resistance was observed for chlorinated hydrocarbons (chloroform) and hydrocarbons (toluene). Moreover, PCA analysis of the sensor response of unmodified graphene showed groupings between chemically similar compounds, and separations between polar and non-polar groups. The hybrid graphene/polymer sensor showed equally if not more, separation between polar/non-polar

groups while also exhibiting unique fingerprints for compounds like DMF and pyridine not evaluated on the unmodified graphene sensor.[23]

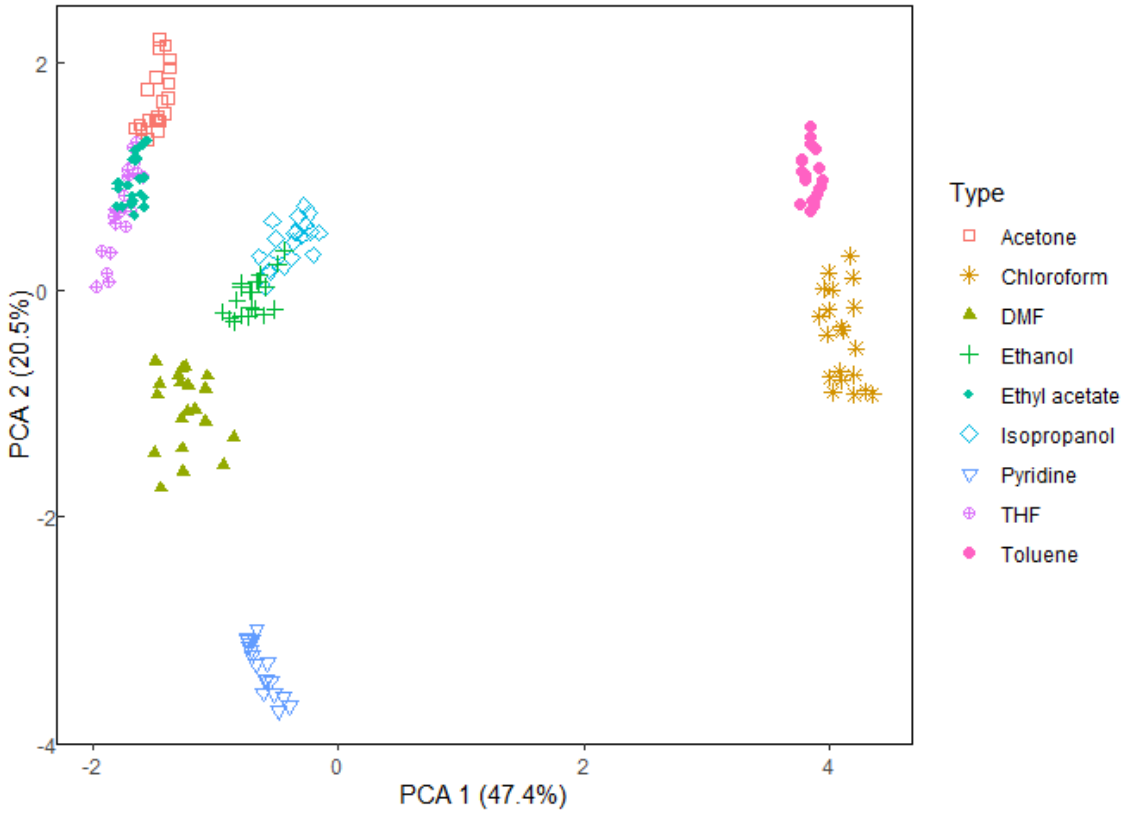

Figure 8. Principal component analysis of the response of an array of graphene polymer hybrid suspended on a textured electrode. The responses showed a clear separation between polar and non-polar analyte vapors. Although much less distinction was present between acetone, ethyl acetate and THF, good separation was observed between aprotic and protic polar VOCs.

The response of the strain sensors was in relation to the number of available columns it was suspended on as shown in figure 5, with signal increasing with increasing number of available columns. This plateau in figure 6b seems to imply the limited degree of strain that

an analyte can impose on the PEVA/Gr. The observed response also seemed to be dependent on other various parameters such as polymer thickness (Figure 4) where optimal thickness was about 70 nm, and the optimal spacing between the columns was obtained using 3 μm diameter and 7 μm pitch mask. Although the signal degraded with time, the sensors exhibited extremely reproducible responses whiling showing facile recovery over numerous extended exposures (x100). However, the hybrid graphene/polymer arrays required a lengthy recovery time of at least 300s to return to their initial signal (Figure 2, 6).

Conclusion

Hybrid polymer graphene strain sensor was created by integrating a simple 3-D pillar electrode to produce a large chemiresistive response to various VOCs of interest. Hybrid materials can allow for the versatile tailoring of novel functionalities of 2 materials combined for highly sensitive vapor sensors. The sensor response was programmed by varying polymer thickness and the underlying structure of the supporting substrate. The polymer, graphene hybrid sensor was extremely sensitive to THF, acetone and pyridine with consistent reproducibility. However, the sensor had long recovery time requiring an extended exposure of background N_2 to recover its full functionality. Pyridine increasing resistance/sensitivity with greater column height implied greater room to allow for the sensor to expand and contract induces greater chances in resistance. A hybrid graphene/polymer sensor array exhibited clear discrimination between polar, non-polar, aprotic, and protic vapors with unique fingerprints for DMF and pyridine.

Supporting Information

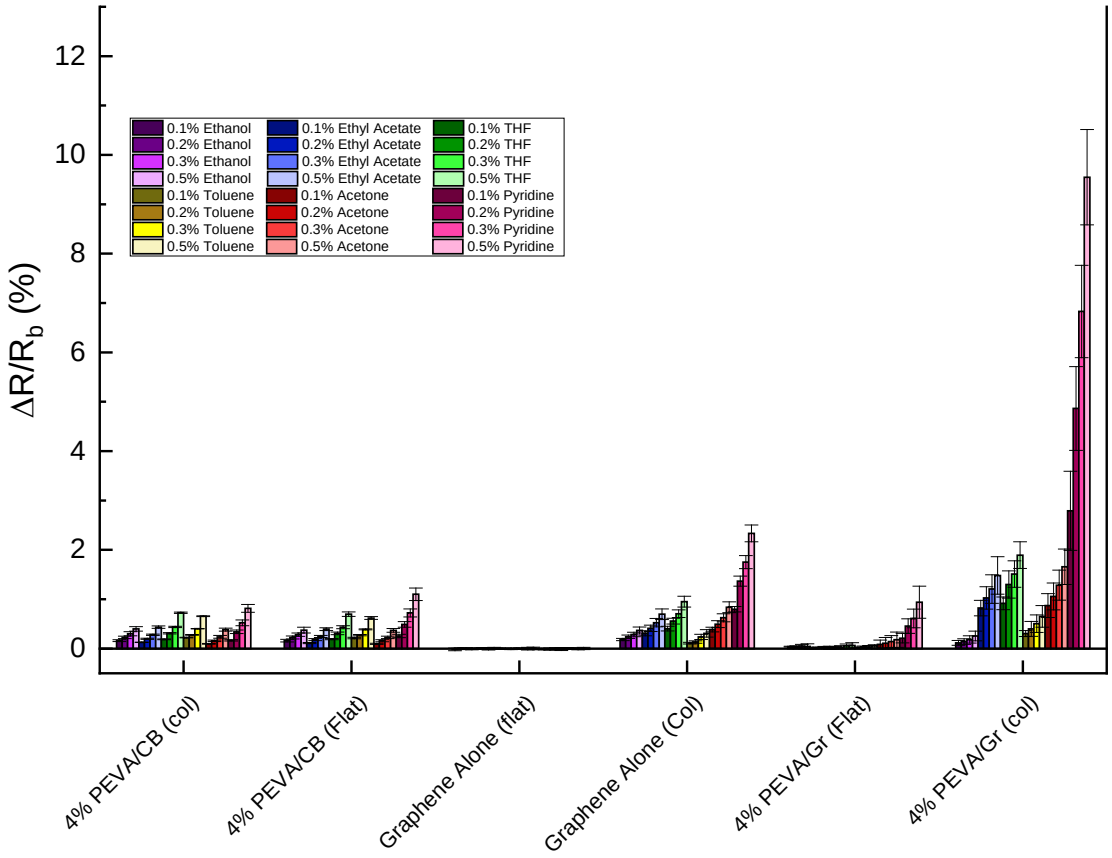

SI 1. Control sensors versus PEVA/Gr on columns (far right) exposed to various VOC partial pressures as a fraction of the analyte vapor pressure (P/P^o) at a flow rate of 3000 ml min^{-1} under N_2 as the carrier gas. The largest $\Delta R_{max}/R_b$ response was observed from the PEVA-graphene film on a glass substrate having 150 nm high columns with a 3 μm diameter and a 7 μm pitch

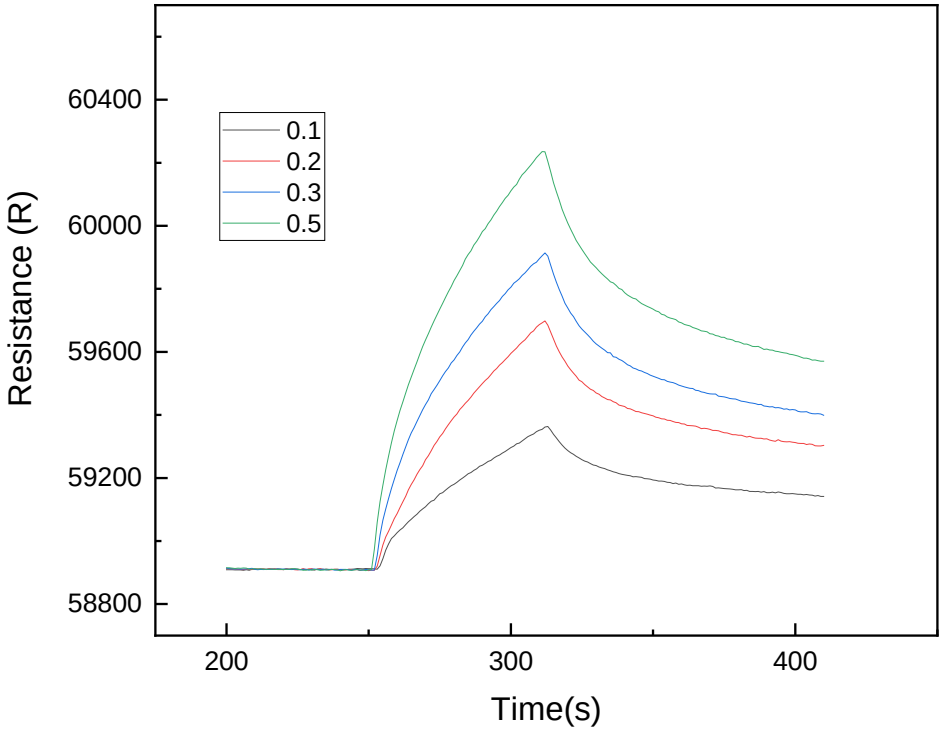

SI 2. Overlay of plain Gr (Col) response curves to single pulses of pyridine at 0.001, 0.002, 0.003, 0.005 P/P^o concentrations. Plain Gr exhibited sharper downturn curve after exposure to VOC suggesting faster recovery vs PEVA/GR (col) as shown in figure 2.

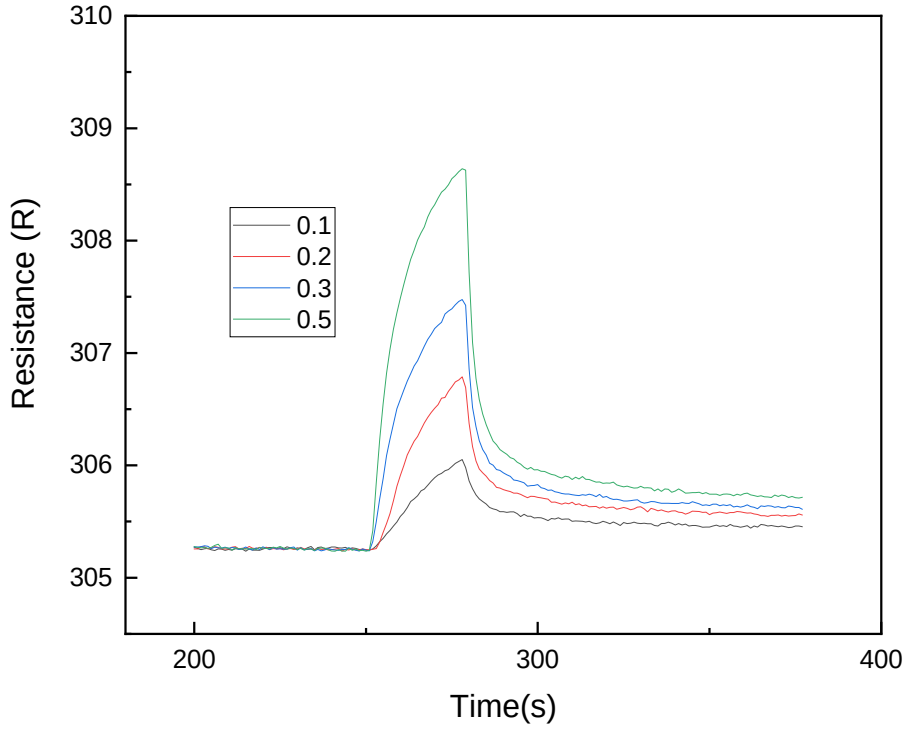

SI 3. Overlay of the 4% PEVA/CB (flat) response curves to a single pulse of pyridine at 0.001, 0.002, 0.003, 0.005 P/P^o concentrations. PEVA/CB (flat) exhibited drastic and fast recovery compared to Gr sensors (S2, Fig 2).

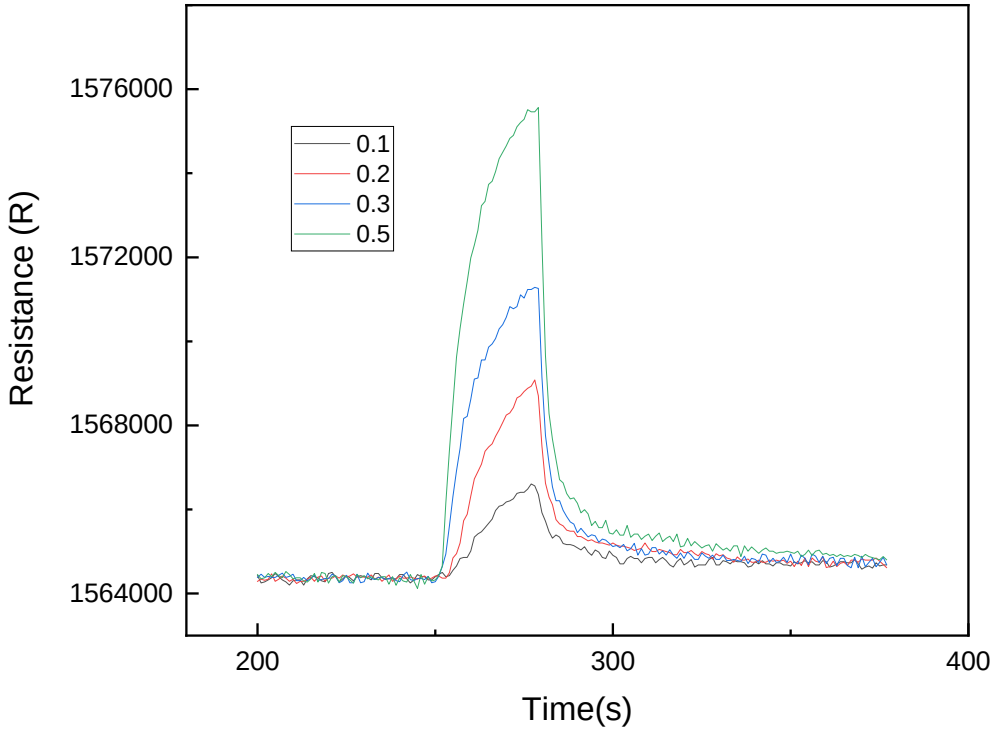

SI 4. Overlay of the 4% PEVA/CB (col) response curves to a single pulse of pyridine at 0.001, 0.002, 0.003, 0.005 P/P^o concentrations. PEVA/CB (col), similar to PEVA/CB (flat) exhibited drastic and fast recovery compared to Gr sensors (S3, S2, Fig 2).

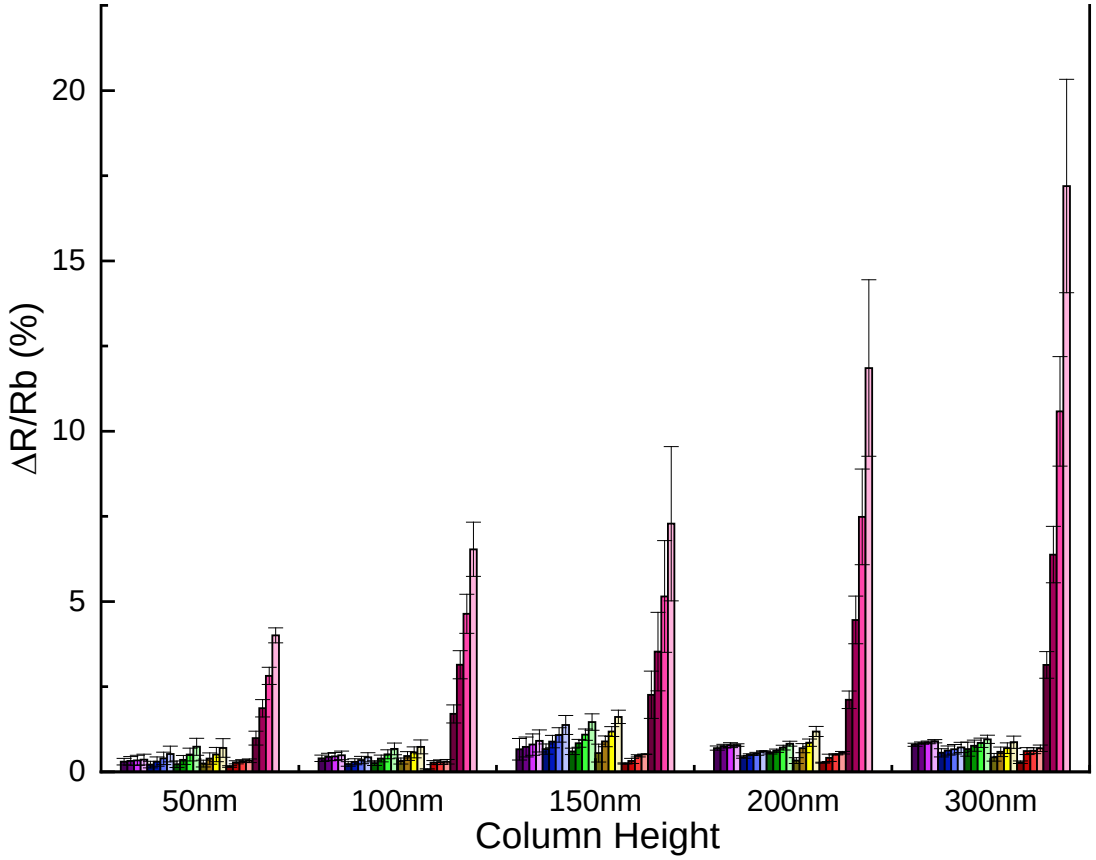

SI 5. Controls for column pillar height for suspended hybrid grapheme sensors exposed to various VOC partial pressures as a fraction of the analyte vapor pressure (P/P^o) at a flow rate of 3000 ml min^{-1} under N_2 as the carrier gas.

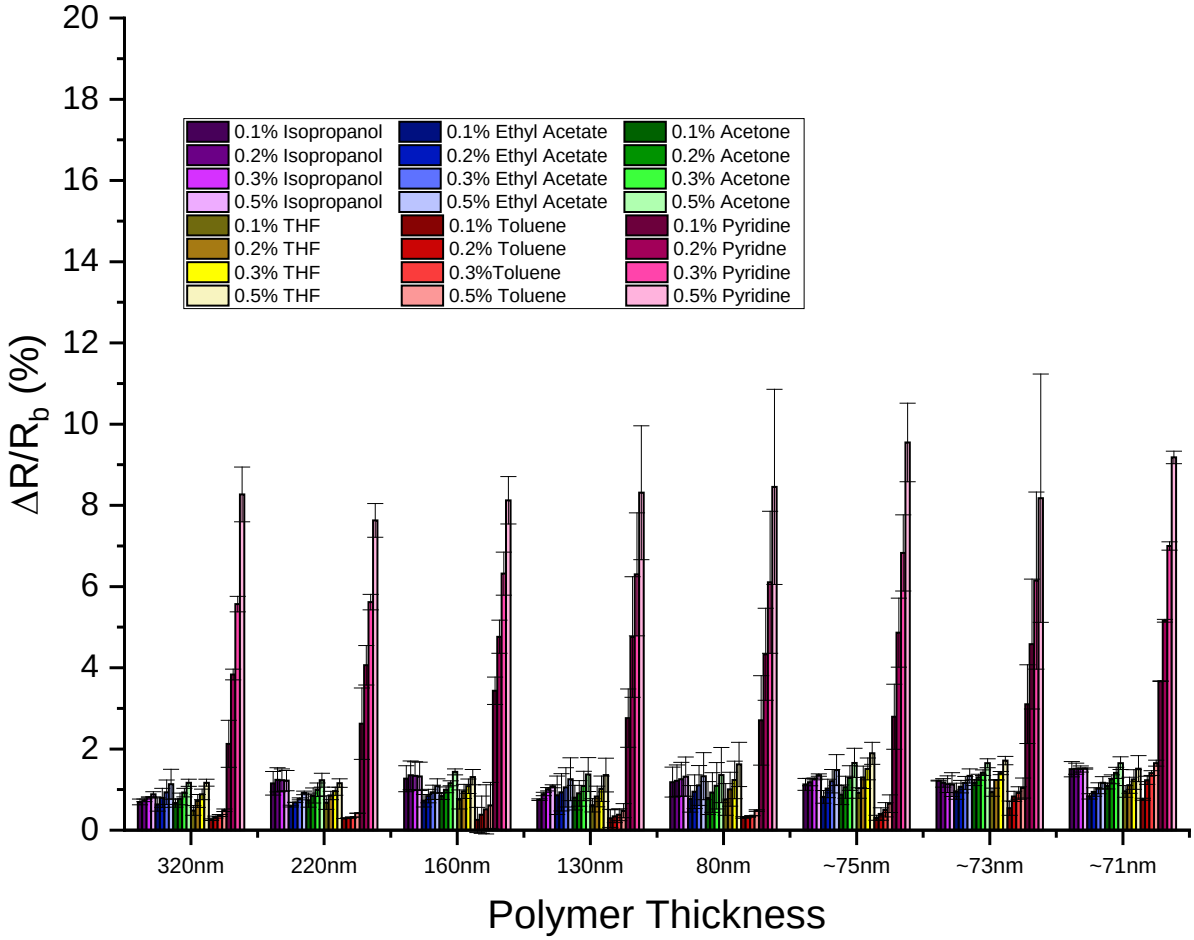

SI 6. Controls for polymer overlayer thickness exposed to various VOC partial pressures as a fraction of the analyte vapor pressure (P/P_o) at a flow rate of 3000ml min^{-1} under N_2 as the carrier gas. The spin speed (rpm) of the polymer thickness was correlated as 1k (320nm), 2k (220nm), 3k (160nm), 4k (130nm), 5k (80nm), 6k (~75nm), 7k (73nm), and 8k (71nm), respectively.

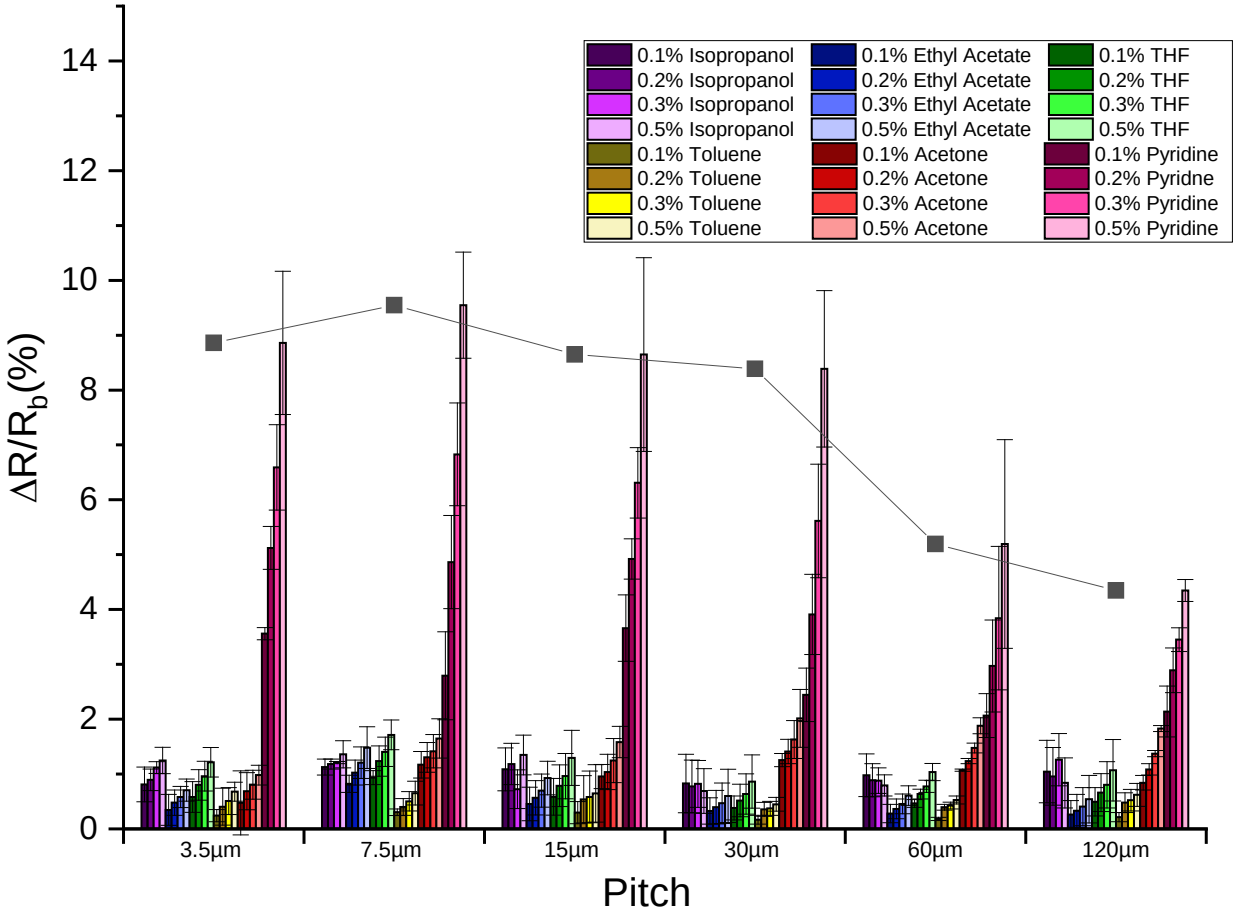

SI 7. Controls for number of columns/pitch of the substrate at various VOC partial pressures as a fraction of the analyte vapor pressure (P/P_o) at a flow rate of 3000 ml min^{-1} under N_2 as the carrier gas.

References

1.Lee, C., Wei, X., Kysar, J. W. & Hone, J. Measurement of the Elastic Properties and Intrinsic Strength of Monolayer Graphene. *Science* **321**, 385–388 (2008).

2.Deng, S. & Berry, V. Wrinkled, rippled and crumpled graphene: an overview of formation mechanism, electronic properties, and applications. *Mater. Today* **19**, 197–212 (2016).

3.Chen, W. *et al.* Controllable Fabrication of Large-Area Wrinkled Graphene on a Solution Surface. *ACS Appl. Mater. Interfaces* **8**, 10977–10984 (2016).

4.Jung, W.-B., Cho, K. M., Lee, W.-K., Odom, T. W. & Jung, H.-T. Universal Method for Creating Hierarchical Wrinkles on Thin-Film Surfaces. *ACS Appl. Mater. Interfaces* **10**, 1347–1355 (2018).

5.Doleman, B. J., Lonergan, M. C., Severin, E. J., Vaid, T. P. & Lewis, N. S. Quantitative study of the resolving power of arrays of carbon black-polymer composites in various vapor-sensing tasks. *Anal. Chem.* **70**, 4177–4190 (1998).

6.Ferrari, A. C. *et al.* Raman Spectrum of Graphene and Graphene Layers. *Phys. Rev. Lett.* **97**, 187401 (2006).

7.Bissett, M. A., Tsuji, M. & Ago, H. Strain engineering the properties of graphene and other two-dimensional crystals. *Phys. Chem. Chem. Phys.* **16**, 11124–11138 (2014).

8.Beams, R., Gustavo Cançado, L. & Novotny, L. Raman characterization of defects and dopants in graphene. *J. Phys. Condens. Matter* **27**, 083002 (2015).

9. Gao, T., Woodka, M.D., Brunschwig, B.S., Lewis, N.S. Chemiresistors for Array-Based Vapor Sensing Using Composites of Carbon Black with Low Volatility Organic Molecules. *Chem. Mater*. **2006**, 18, 5193-5202

10. E. Garcia-Berrios, J. C. Theriot, M. D. Woodka and N. S. Lewis. Detection of ammonia, 2,4,6-trinitrotoluene, and common organic vapors using thin-film carbon black-metalloporphyrin composite chemiresistors. *Sensors and Actuators B Chemical*, **2013** , *188*, 761-767

10. Garcia-Berrios, T. Gao, D. Walker, B. S. Brunschwig and N. S. Lewis. Composites of carboxylate-capped TiO_2 nanoparticles and carbon black as chemiresistive vapor sensors. *Sensors and Actuators B-Chemical*, **2011** , *158*, 17-22

11. Hybrid Materials: Synthesis, Characterization, and Applications. Edited by Guido Kickelbick (Technische Universität Wien, Austria). Wiley-VCH Verlag GmbH & Co. KGaA: Weinheim. 2007. xviii + 498. ISBN 978-3-527-31299-3.

12. Xu. W., Qin, Z. Chen, C., Kwag, H., Ma, Q., Sarkar, A., Buehler, M.J. and Gracias, D.H. Ultrathin thermoresponsive self-folding 3D graphene. *Science Advances,* 2017: Vol. 3, no. 10, e1701084

13. Yi, J., Lee, J.M., Park. W. Vertically-Aligned ZnO Nanorods and Graphene Hybrid Architectures for High-Sensitive Flexible Gas sensors. Sensors and Actuators B Chemical 155(1): 264-269 (2011).

14. Georgalkilas, V., Otyepka, M., Bourlinos, A.B., Chandra, V., Kim, N., Kemp, K.C., Hobza, P., Zboril, R., Kim, K.S. Chem. Rev. 2012, 112, 11, 6156-6214

15. Wang, M., Duan, X., Xu, Y., Duan, X. Functional Three-Dimensional Graphene/Polymer Composites. ACS nano 2016, 10, 8, 7231-7247

16. Gu, J. *et al*. Functionalized graphite nanoplatelets/epoxy resin nanocomposites with high thermal conductivity. *Int. J. Heat Mass Transf.* **92**, 15–22 (2016).

17. Ji, T. *et al*. Thermal conductive and flexible silastic composite based on a hierarchical framework of aligned carbon fibers-carbon nanotubes. *Carbon* **131**, 149–159 (2018).

18. Janaky, C. & Visy, C. Conducting polymer-based hybrid assemblies for electrochemical sensing: a materials science perspective. *Anal. Bioanal. Chem.* **405**, 3489–3511 (2013).

19. Reina, A.; Jia, X.; Ho, J.; Nezich, D.; Son, H.; Bulovic, V.; Dresselhaus, M. S.; Kong, J. Nano Lett. 2009, 9, 30

20. Ponnamma, D., Guo, Q., Krupa, I., Al-Maadeed, M.S., Varughese, K.T., Thomas, S., Sadasivuni, K.K. Graphene and Graphitic Derivative filled Polymer Composites as potential sensors**.** ***Phys. Chem. Chem. Phys.***, 2015,**17,** 3954-3981

21. Wang C. A Novel Method for the Fabrication of High-Aspect Ratio C-MEMS Structures. J. Microelectromech. Syst. 2005;14:348–358. doi: 10.1109/JMEMS.2004.839312.

22. Hemanth, S., Caviglia, C., Keller, S.S. Suspended 3D pyrolytic carbon microelectrodes for electrochemistry**.** Carbon, Vol 121, 226-234, 2017

23. Nallon, E.C., Schnee, V.P., Bright, C., Polcha, M.P., Li, Q. Chemical Discrimination with an unmodified Graphene chemical sensor. *ACS Sensors*, 2015, 1, 26-31.

Chapter 2

FUNCTIONALIZED MOS_2 SENSORS

Introduction

Artificial olfactory systems, or electronic noses, has for several years attracted great interest for several applications such as air quality checking, disease diagnostics, and etc. Based on an array of cross-reactive, chemically sensitive resistive sensors provide a simple technological implementation of a vapor detection by mimicking the functionality of biological olfactory systems. When exposed to volatile organic vapors, the analyte permeates and reacts with the sensing material, producing a change in dc resistance. Different vapors are recognized and classified using pattern recognition algorithms and a neural network. [9,10,11] Previous electronic nose sensors were developed using a variety of materials such as intrinsically conducting or non-conducting polymers loaded with conducting material such as carbon black and graphene, as well as individually functionalized metallic nanoparticles and other related systems.

2-D materials sparked a tremendous wave of interest and research efforts due to their tremendous potential. Graphene holds unique electronic properties while also exhibiting power mechanical properties such as remarkable flexibility and strength, however due the nature of graphene and its gapless band gap and inert chemical nature, certain applications are limited.[1,3, 4] Therefore, researchers have pushed for exploration of other possible 2-D materials, one such material being transition metal dichalcogenides (TMDCs). TMDCs are

similar to graphene offering tremendous potential in a wide variety of electronic applications such as sensors, photovoltaics, batteries and etc.[7,8] Particularly, MoS_2 has attracted immense attention particularly due to its unique electronic and surface properties. One such unique behavior is due to its charge carriers.[2,6] MoS_2 are Van der waals solids, where the quantum restriction and the changes in its interlayers results in the unique differences in the properties of a single layer of MoS_2 vs a few/multiple layers of MoS_2. Strong intralayer bonding with weak interlayer bonding leads to changes in the band-gap behavior in bulk vs. monolayers of MoS_2. Bulk TMDC has an indirect band gap of ~1.2eV, while monolayer MoS_2 has a direct band gap of ~1.8eV and comes in various types, the 2H phase and IT phase.[1,6] Remarkably, 2H (hexagonal) phase is thermodynamically stable and semiconducting and 1T(trigonal prismatic) phase is metastable metallic. Its crystal structure is composed of layers of S-Mo-S held together by van der waals forces. The focus of this chapter is on functionalized IT phase MoS_2.

There are also various procedures to obtain monolayer nanosheets of MoS_2, where nanosheets can be obtained through exfoliation from bulk material in either 2H phase or 1T phase.[3,5] Mechanical, chemical, liquid or CVD/thermal exfoliation can be used to obtain monolayers but these each method has its advantages and disadvantages. Mechanical exfoliation offers high quality mono-layers suitable for high performance devices, however, it yields are poor limiting it to short-scale production.[1,7] Liquid/ultrasonification offers higher yields in comparison however by overcoming the van der waals bonds between the layers it can have undesired effects such as breaking of nanosheets to result in low yields of monolayers. Chemical exfoliation is a good option for mass production, however, semiconducting 2H phase coverts to metallic 1T-phase after lithium intercalcation. The

converted IT-phase is still very unstable and again reverts back to 2H phase.[3,6] Chemical exfoliation was mainly used in this work.

Various 2-D materials such as graphene offer low detection limits especially with small organic vapors such as methanol, and THF, where different chemical vapor molecules induce different behaviors and noise within the sensing 2-D material.[1,2,5] And functionalization of these 2-D materials offers even more numerous possibilities by not only allowing for tailoring of electronic and optical properties for numerous applications but also increasing its' stability. As sensors, stacked functionalized MoS_2 results in increased surface area and pore volume specifically enhancing its gas sequestering properties which can be designed for novel chemical gas sensing properties.[5,6]

Functionalization can be performed through non-covalent or covalent interactions, but each method has its advantages and disadvantages. Covalent modification forms strong bonds onto the interface due to its strong hybridization of orbitals and thus allow for potential altering of its electronic properties. Non-covalent functionalization offers weak bonding at the surface due to its weak interaction with the orbitals but does preserve the electronic properties within the materials. However, like graphene, TMDs are chemically inert, making covalent modifications extremely difficult.[5] Previous research has used vacancies/defects/edges within the TMDs material to functionalize its surface because no material is perfectly coordinated. Specifically, MoS_2 displays sulfur vacancies acting as reactive centers which provides useful means to tweak its surface. However, using sulfur vacancies and defects limits available coverage where most literature reports less than 35% surface coverage. Furthermore, covalent functionalization is typically limited to a maximum coverage of 25-27% due to 1T phase MoS_2 limited storage of negative charges from lithium

intercalation. However recent work by the Lewis Group has achieved increased surface functionalization through usage of reductants.[6,9] This work uses the method achieved by the Lewis group to use reductant-activated functionalized MoS_2 as sensitive, robust sensors for the detection of VOCs. Specifically, this work uses a one-electron metallocene reductant (nickelocene, cobaltocene, or octamethyl nickelocene) along with methyl/propyl halides during the functionalization reaction enabling these weak electrophiles, typically unreactive with the inert surface of exfoliated MoS_2, to achieve covalent bonding. Through this, we not only observe that by adding a sufficiently strong one-electron reductant, we can increase the coverage of functional groups beyond the previous limit, but also use the increased coverage for the sensitive detection of VOCs on the electronic nose.[9]

Methods

Materials

All solvents including n-butyllithium (in hexanes) and bis(cyclopentadienyl) cobalt (II) (cobaltocene) were from VWR and Sigma Aldrich, all of which was used as needed without need for further purification. Molybdenum disulfide powder (99%), bis(tetramethylcyclopentadienyl) nickel (II) (octamethylnickelocene), bis(cyclopentadienyl) nickel (II) (nickelocene) were obtained from Sigma Aldrich. All chemicals listed thus far was stored in Argon in a glove box (<1 ppm O_2). Nanopure water was obtained from Nanopure E-Pure system at > 18.2 MΩ·cm.[9]

Synthesis of chemically exfoliated MoS2

400mg of MoS2 (99%) was heated with 4ml of n-butyllithium (conc. Of 1.6M in hexanes) for 46 hrs in a sealed glass tube. Afterward the MoS_2 was filtered and washed with 20mL of anhydrous hexanes, then exfoliated in 180 ml of nanopure water. The suspension was sonicated for 1hr than centrifuged at 2000 rpm for 5min to remove unexfoliated material. The supernatant was collected and washed repeatedly with H_2O and was then washed with anhydrous DMF until clear. The final product was resuspended in 2:1 water/isopropanol or DMF, usually kept at a concentration of 2mg/ml. Samples were characterized by XPS and with ATR-FTIR and NMR measurements.[9]

Functionalization of IT'-MoS_2

The chemically exfoliated MoS_2 was functionalized in DMF where the end groups such as alkyl halides were added 10-fold and stirred for 42hrs, completely covered in tin foil. The reaction was than centrifuged and washed at 6000rpm for 30min where the precipitate was collected and resuspended and rewashed 3x. The final product was washed with isopropanol, methanol, and nanopure water. The final product was characterized by XPS and the solvent was removed in vacuum, obtaining the final dry powder.[9]

Reductant activated functionalized MoS_2

The already functionalized of MoS_2 was suspended in 10ml of DMF and the same end group was added 10-fold. Ferrocene was added in ambient conditions, while nickelocene, octamethylnickelocene, cobaltocene was added in an Ar-glovebox. The solution was stirred for 66hrs where the reaction was covered completely in foil. The end reaction was purified through centrifugation at 6500rpm for 10min and resuspended through sonication and washed with DMF for 3-4 rounds, until the color of the metallocene was not visible. Then

the product was washed with 24ml of isopropanol and 24 ml of methanol. The final product was characterized using XPS and final dry product was obtained through removal of solvent through vacuum.[9]

Sensor creation

Redispersion of the functionalized samples for electrode placement was conducted using 1.3-1.5 mg of respective material immersed in 2.6-3.0 ml of the respective solvent to bring the nanomaterial concentration to 0.5 g/L. The dispersed samples were sonicated for 20min (Bandelin, Sonorex Digital 10P, DK 255 P, 640 W) before it was drop casted onto the interdigitated electrodes. The baseline resistance varied by volume of sample used and was placed in the gas-tight vapor testing chamber.

Vapor testing

Sensors were tested using a custom setup that has been described previously N_2(g) was used as a carrier gas through the bubblers at a flow rate of 3000 mL/min. Organic vapors were generated by sparging N_2(g) through 45 cm tall bubblers that had been filled with the appropriate solvents.[9] The analyte concentration was controlled by adjusting the volumetric mixing ratio of the saturated analyte stream to the background N_2(g) stream. The flow rates of the background and analyte gases were regulated using mass flow controllers. Each run started with a 700 s background collection. Each analyte exposure consisted of 300 s of pure background gas, 80 s of diluted analyte, and then 300 s of background gas to purge the system at a flow rate of 3000ml/min. The sensors were loaded into a rectangular, 16-slot chamber

connected by Teflon tubing to the gas delivery system. The resistance of each of the sensors in the array was measured by a Keysight technologies 34970A data acquisition/switch unit with Keysight 34903A 20 Channel Actuator. The measurement electronics were interfaced with a computer via a GPIB connection and were controlled with LabVIEW software.

All data processing was conducted through custom-routines in Matlab, where a resistance-baseline was calculated as $\Delta R_{max}/R_b$, where Rmax is the baseline corrected response maximum upon VOC exposure to the sensor, and where R_b is the baseline resistance under just inert N_2. A spline was best-fitted where the values of $\Delta R_{max}/R_b$ was calculated by subtracting the values of the spline over the deduced exposure time with its observed resistance during the length of exposure.

Results

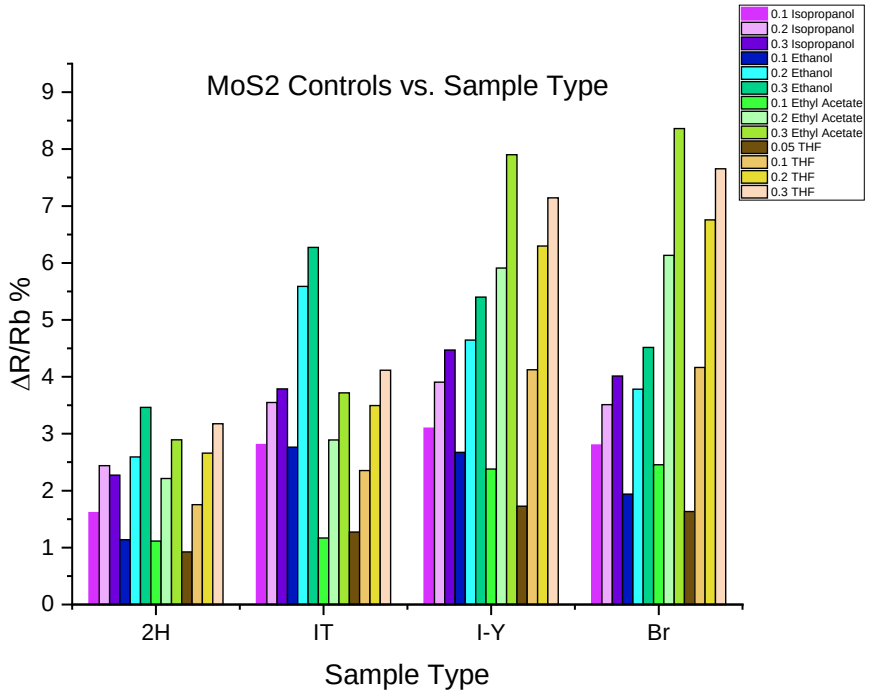

Figure 1. MoS_2 controls (2H and IT type MoS2) vs. Iodo-2-methyl propane and bromopentane. Both controls were obtained by intercalation.

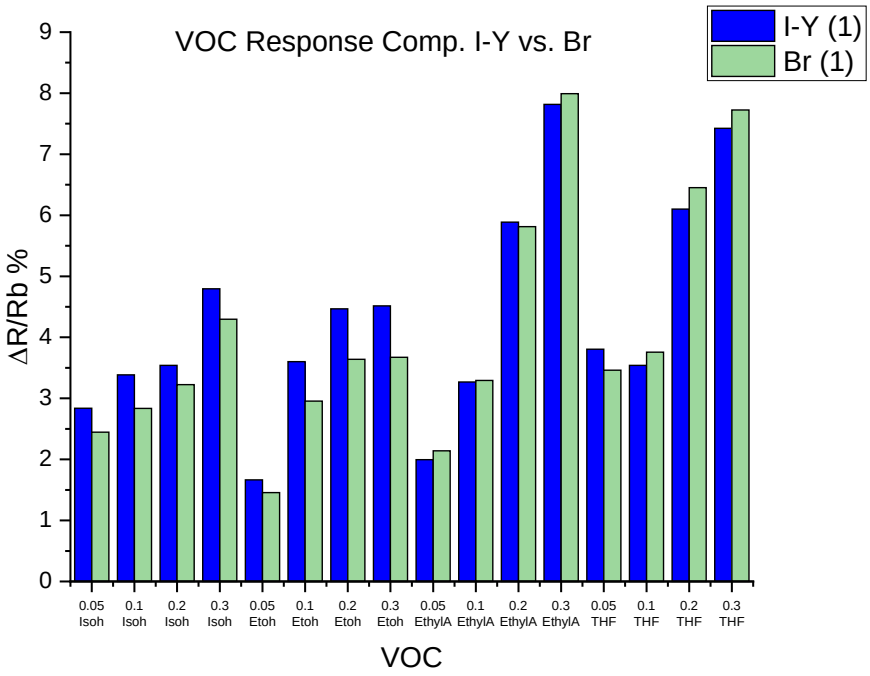

Figure 2. A closer side-by side comparison at the slight difference in varying alkane chain lengths/nucleophile of iodo-2-methyl propane and bromopentane..

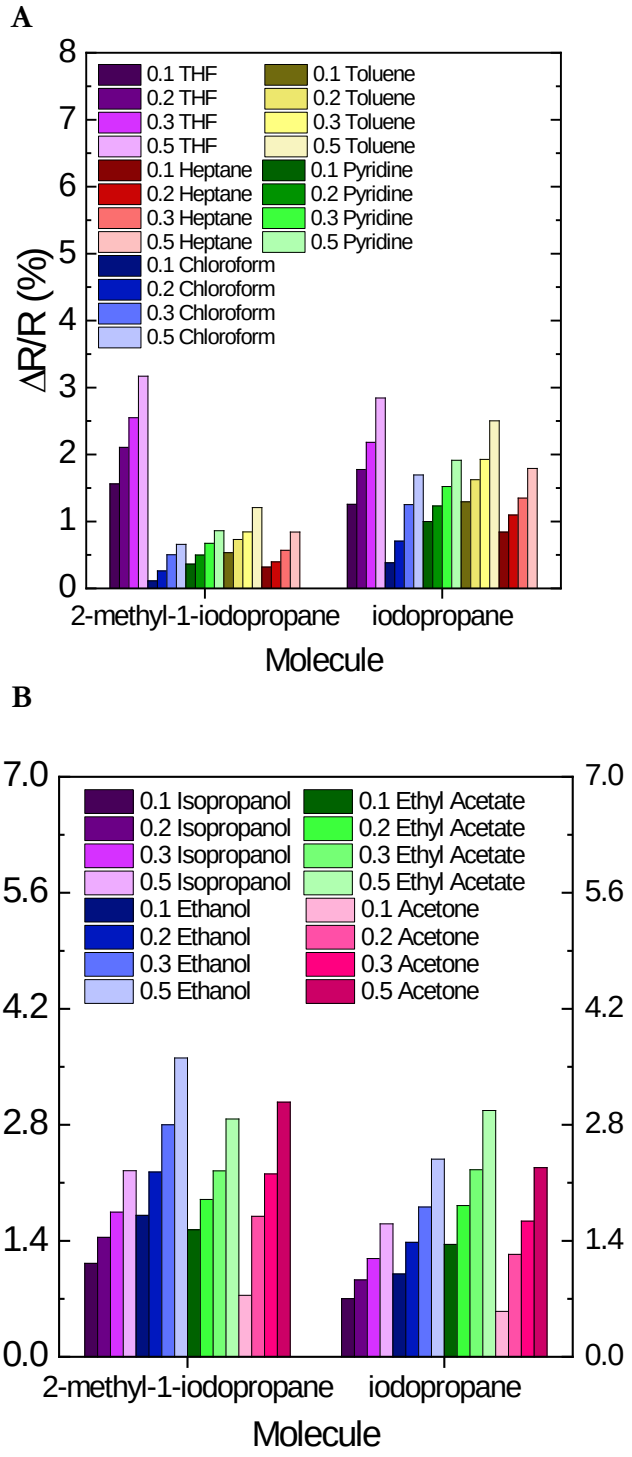

Figure 3. A) Comparison look at alkane non-polar functional groups- 1 branched (2-methyl-1-iodopropane), 1 straight chain (iodopropane). Branched 2-methyl-1-iodopropane exhibits

lower signal than straight chained with nonpolar VOCs. B) Comparison look at alkane non-polar functional groups- 1 branched, 1 straight chain. Branched alkane groups exhibits slightly higher signal compared to it straight chain counter-part for polar VOCs.

A

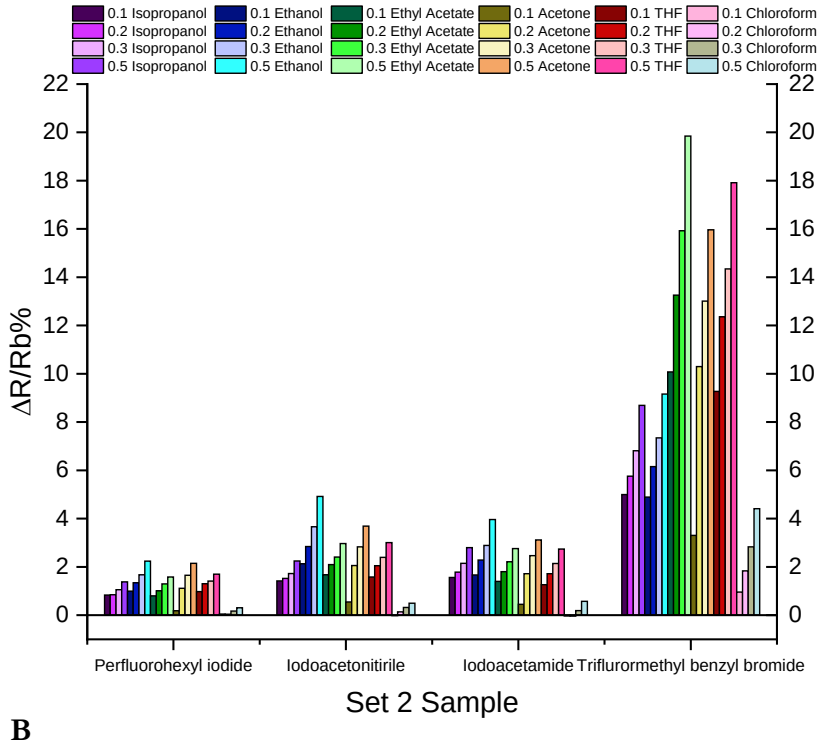
0.1 Isopropanol
0.2 Isopropanol
0.3 Isopropanol
0.5 Isopropanol
0.1 Ethanol
0.2 Ethanol
0.3 Ethanol
0.5 Ethanol
0.1 Ethyl Acetate
0.2 Ethyl Acetate
0.3 Ethyl Acetate
0.5 Ethyl Acetate
0.1 Acetone
0.2 Acetone
0.3 Acetone
0.5 Acetone
0.1 THF
0.2 THF
0.3 THF
0.5 THF
0.1 Chloroform
0.2 Chloroform
0.3 Chloroform
0.5 Chloroform
ΔR/Rb%
0
2
4
6
8
10
12
14
16
18
20
22
Perfluorohexyl iodide
Iodoacetonitirile
Iodoacetamide
Triflurormethyl benzyl bromide
Set 2 Sample

B

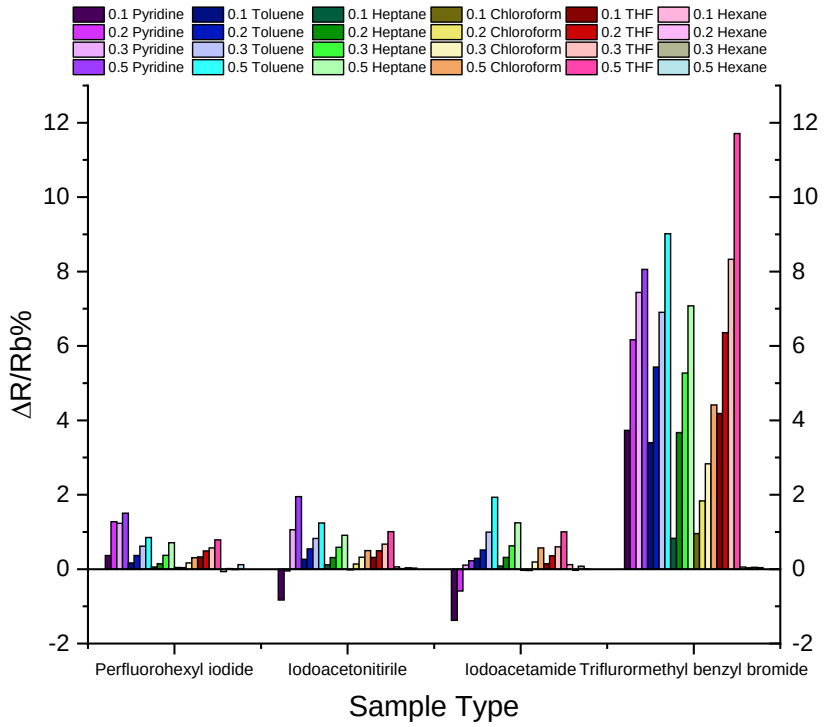
0.1 Pyridine
0.2 Pyridine
0.3 Pyridine
0.5 Pyridine
0.1 Toluene
0.2 Toluene
0.3 Toluene
0.5 Toluene
0.1 Heptane
0.2 Heptane
0.3 Heptane
0.5 Heptane
0.1 Chloroform
0.2 Chloroform
0.3 Chloroform
0.5 Chloroform
0.1 THF
0.2 THF
0.3 THF
0.5 THF
0.1 Hexane
0.2 Hexane
0.3 Hexane
0.5 Hexane
ΔR/Rb%
-2
0
2
4
6
8
10
12
Perfluorohexyl iodide
Iodoacetonitirile
Iodoacetamide
Triflurormethyl benzyl bromide
Sample Type

Figure 4. A) Overall look at polar functional groups (iodoacetonitrile, iodoacetamide, 4-trifluoromethylbenzyl bromide) exposed to more non-polar VOCs (THF for polar VOC comparison). Lower signal for was observed for non-polar VOCs compared to when exposed to polar VOCs in 5b. B) Overall look at polar functional groups (iodoacetonitrile, iodoacetamide, 4-trifluoromethylbenzyl bromide) exposed to more polar VOCs. 4-trifluoromethylbenzyl bromide had almost 2x the signal of other polar functional MoS_2 groups.

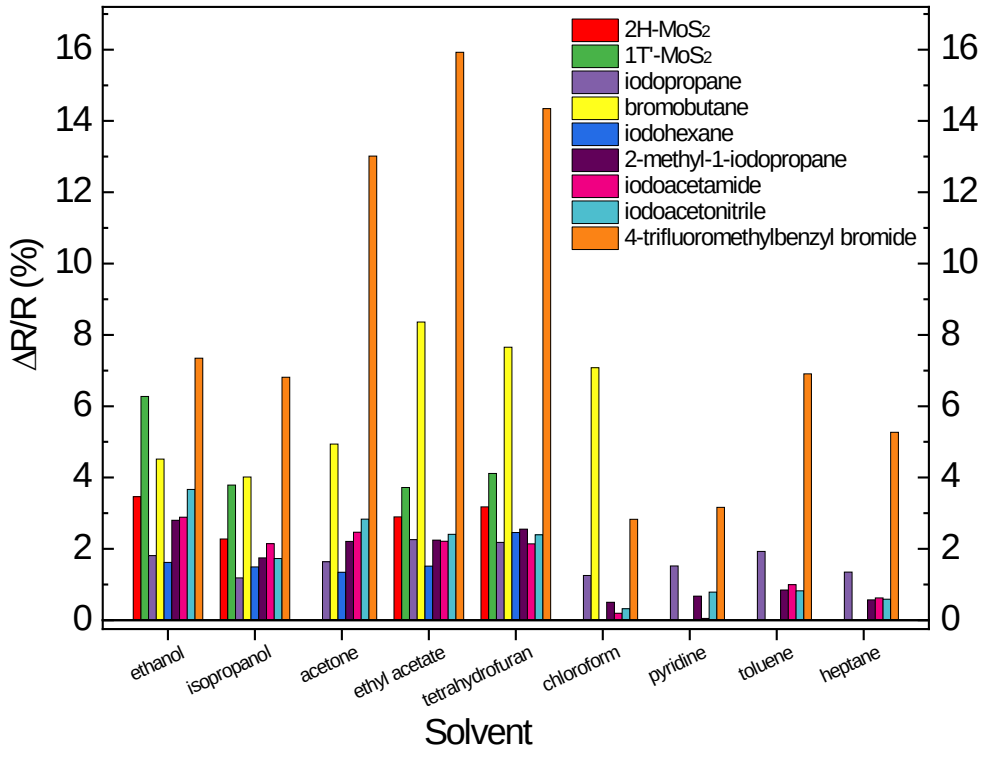

Figure 5. Functionalized MoS_2 (2H and IT) controls behaved very differently from their functionalized counterparts. Samples exhibited lower response to non-polar VOCs.

MoS_2 controls (2H and IT) were only exposed to ethanol, isopropanol, acetone, ethyl acetate, and THF. Iodohexane was not exposed to chloroform, pyridine, toluene and heptane.

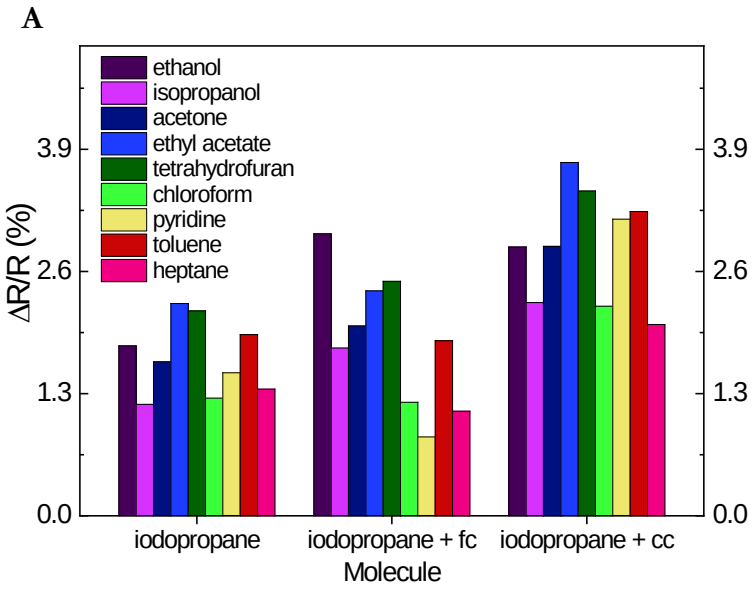

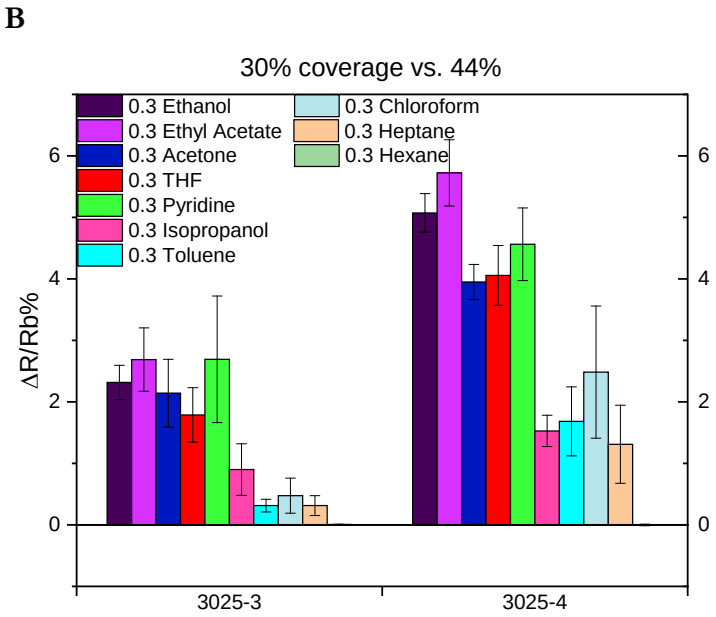

Figure 6. A). Comparison on how varying reductants in the synthesis of the functionalized MoS_2 sheets will change the chemi-resistive behavior of the MoS_2 sensors. Coverage for fc and cc were similar at about 40% while no reductant used (iodopropane) had a coverage of 28%. Resistance increased with reductant addition. Addition of ferrocene (FC) does not seem to increase the response of non-polar VOCs. However, cobaltocene (CC) response increased for all VOCs. B). Increased functionalization coverage due to reductant usage in the synthesis does increase the response.

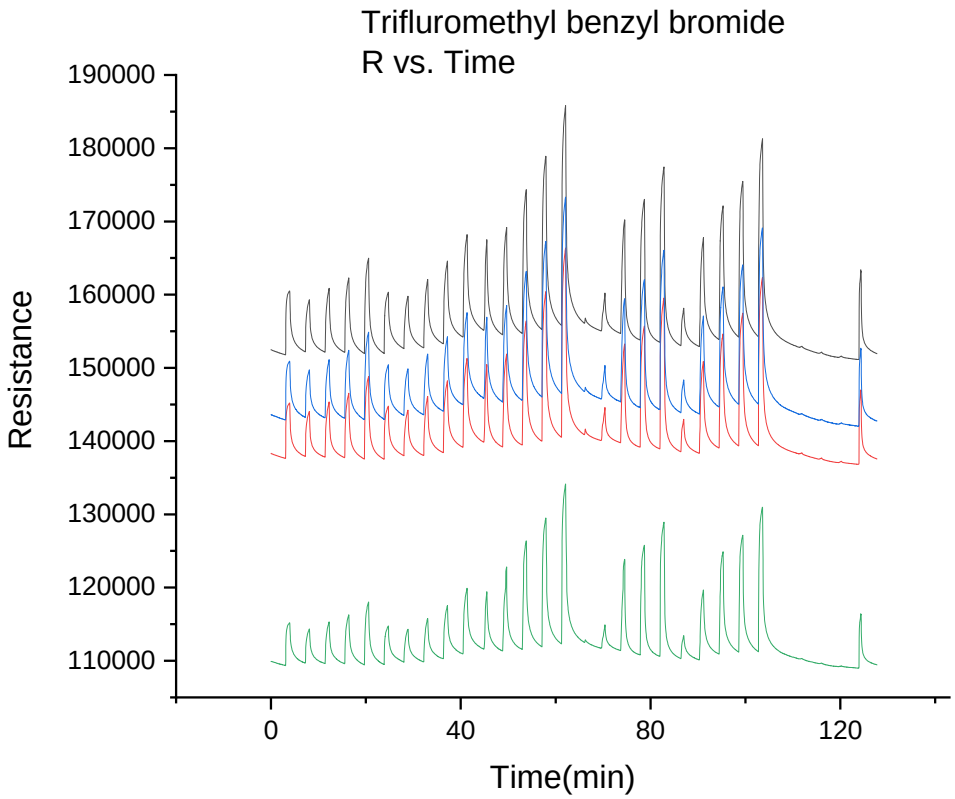

Figure 7. Curve behavior of 4 samples of trifluoromethyl benzyl bromide f-MoS_2 to various VOC exposures at a nitrogen carrier gas flow rate of 300ml min^{-1}). Exposures does completely recover completely given at least 300s of rest under inert nitrogen (flow rate of 3000 ml min^{-1}).

A

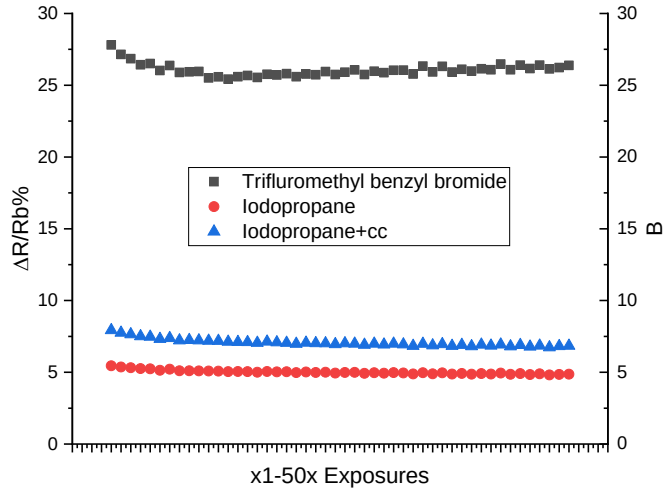

B

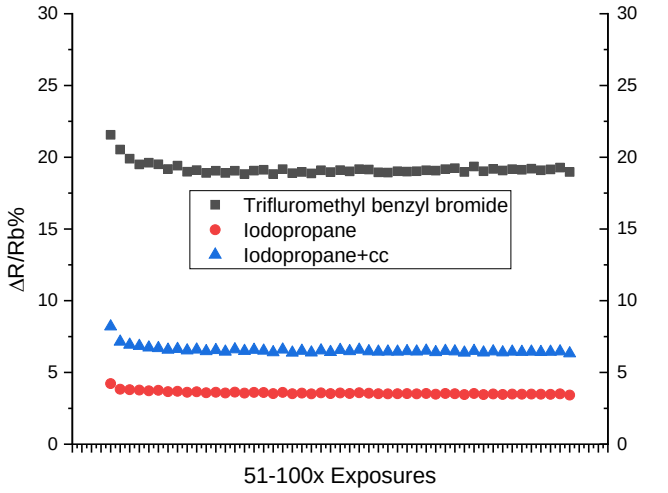

Figure 8. A). Optimized 50 repeated exposures to ethyl acetate response at $P/P^o = 0.0050$ (nitrogen carrier gas at a flow rate of 3000 ml min^{-1}) showing reproducability with 300s of rest (N_2) in between exposures to both trifluromethyl benzyl bromide, iodopropane and iodopropane+cc. B) Comparison of exposures after 72hrs of rest where the samples were exposed to 50 more repeated ethyl acetate exposures at $P/P^o = 0.0050$ (nitrogen carrier gas at a flow rate of 3000 ml min^{-1}) (black). Response all across the board was lowered after rest.

Discussion

Initially four different VOCs (5 polar: Isopropanol, Ethanol, Ethyl Acetate, THF) were exposed to 2 MoS_2 controls (2H phase and IT phase) and 2 MoS_2 alkane functionalized (Iodo-2-methylpropane and bromopentane) as shown in Figure 1. 2H phase had the smallest response to the polar analytes while for IT phase, alcohol groups performed just as well if not better than the functionalized alkane MoS_2 groups while the functionalized MoS_2 (f-MoS2) exhibited higher response for ethyl acetate and THF. A closer look at the VOC response to the two f-MoS_2 was compared where iodo-2methyl propane had a slightly higher but similar response compared to bromopentane for alcohols, but bromopentane had similar but higher response for ethyl acetate and THF.

Due to the initial result, various different VOCs (3-4 non-polar, 6 polar), at 4 different concentrations (0.1%, 0.2%, 0.3%, and 0.5% P/P) were exposed to 6 different f-MoS_2 (2 non-polar functional end groups, 4 polar functional end groups, Figure 9) as shown in Figure 3 and 4. All responses showed linearity in behavior with increasing VOC concentration exemplifying the potential fidelity of the sensor. Non-polar vapors exhibited lower signal compared to polar VOCs for all the different types f-MoS_2 as shown in figure 5. The greatest

signal was observed from the trifluoromethyl benzyl bromide MoS_2 sensor. Ethanol and ethyl acetate traditionally had the highest responses, while hexane and chloroform sensitivity were poor for most sensors. In Figure 3, 2 alkane non-polar functional groups (1 branched (2-methyl-1-iodopropane) , 1 straight chain (iodopropane)) were compared where branched alkanes exhibited lower response than straight chain to non-polar VOCs while branched exhibited higher response than straight chain to polar VOCs.

Non-polar functional groups

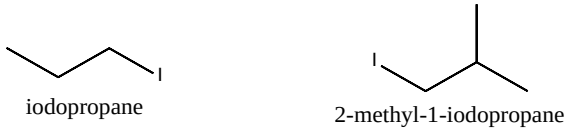

iodopropane 2-methyl-1-iodopropane

Polar functional groups

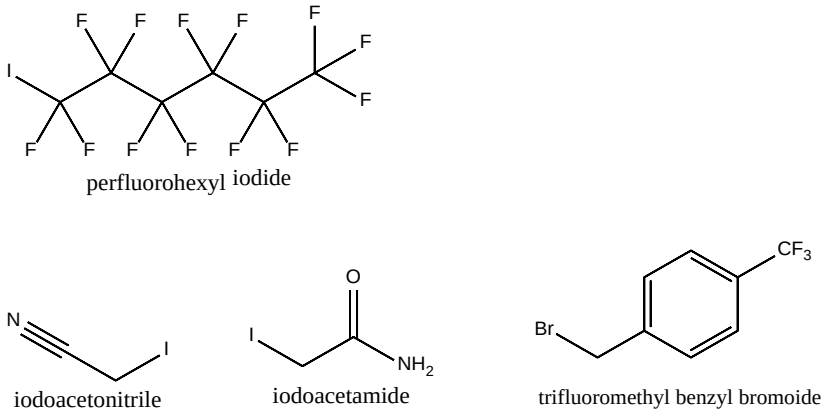

perfluorohexyl iodide

iodoacetonitrile iodoacetamide trifluoromethyl benzyl bromoide

Figure 9. Chemical structure of the 6 various f-MoS2 tested, 2 non-polar, 4 polar.

Figure 4 compares the VOC exposures to polar f-MoS2. Iodoacetonitrile and iodoacetamide exhibited an interesting response to pyridine initially showing a negative response but increased in resistance as concentration of pyridine exposure increased. Hexane

signal was extremely poor and unstable, sometimes exhibiting negative signal (<0.5% $\Delta R/R_b$). Overall perfluorohexyl iodide exhibited the lowest signal even compared to the non-polar f-MoS2 sensors. The trifluoromethyl bromide exhibited the greatest signal, performing at least 2-fold better than all other f-MoS2 sensors as shown in figure 5.

Comparison on varying the type of reductants used to increase functionalization was also tested as shown in Fig 6. Coverage for FC and CC were similar at around 40% while no reductant used had about a 28% coverage. Figure 6a showed slightly higher response for cc compared to fc while iodopropane with no reductant usage showed the lowest polar response. Addition of ferrocene (FC) does not seem to increase the response of non-polar VOCs compared to no reductant used. However, cobaltocene (CC) response increased for all VOCs. However, no reductant iodopropane could have had a lower response due to lower coverage because lower coverage was associated with lower response as shown in 6b. Figure 7 presents the curve behavior of f-MOS_2. The sensors did recover completely however prolonged rest time (at least 300s) in between exposures was needed. Typically, polymer sensors and the graphene strain sensor required less than 200s of rest time.

Figure 8 shows consistent stability in response when f-MoS_2 (trifluoromethyl benzyl bromide, iodopropane and iodopropane+cc) sensors were exposed to multiple repeated exposures. However, after 72hrs of rest (fig. 8b), although all 3 types of f-MoS_2 sensor exhibited consistent response when exposed to 50x ethyl acetate exposures, all 3 sensors exhibited lower resistance change after the 72hrs of rest. When the electrodes were further examined it was found that the 3 sensors had higher baseline resistance compared to when they were tested 72hrs earlier. It was proposed that stability and sensitivity falls as the sensor ages.

Conclusion

This was just the preliminary work for f-MoS_2 sensors for the sensitive detection of VOCs. These sensors shows incredible sensitivity, out performing many previous polymer and 2-D material sensors for polar VOCs. Different functionalized groups showed varied, large responses to different VOCs. The greatest signal was observed from the trifluoromethyl benzyl bromide MoS_2 sensor (showing consistent response for ethyl acetate as high as >20% $\Delta R_{max}/R_b$.), where ethanol and ethyl acetate traditionally had the highest responses, while hexane and chloroform sensitivity were poor for most sensors. Responses also changed due to type of reductant used and coverage. Future work needs to be conducted on standardization experiments involving coverage and types of reductant used effects on the sensors along with PCA/discrimination studies to see how well the sensor discriminates between the various VOCs.

References

1. Stergiou, A., Tagmatarchis N. Molecular Funcitonalization of Two-Dimensional MoS2 Nanosheets. *Chemistry Europe* **24**, 18246-18257 (2018).

2. Presolski S., Pumera M. Covalent functionalization of MoS_2. *Materials Today* 19(3), 140-145 (2016).

3. Pham, T., Li G., Bekyarova E., Itkis, M.E., Mulchandani A. MoS_2- Based optoelectronic gas sensor with sub-parts-per-billion Limit of NO_2 Gas detection. *ACS Nano* 13, 3196-3205 (2019).

4. Chen, Y., Tan, C., Zhang, H., Wang, L. Two-dimensional graphene analogues for biomedical applications. Chem, Soc. Rev. 44, 2681-2701 (2015).

5. Voiry, D., Goswami, A., Kappera, R., Carvalho, C., Kaplan, D., Fujita, T., Chen, M., Asefa, T., Chhowalla, M. Covalent Functionalization of Monolayered Transition Metal Dichalcogenides by Phase Engineering. *Nat Chem*. 7, 45-49 (2015).

6. Knirsch, K.C., et al. Basal-Plane functionalization of chemically exfoliate molybdenum disulfide by diazonium salts. *ACS Nano* 9, 6018-6030 (2015).

7. Wang, Q. H., Kalantar-Zadeh, K., Kis, A., Coleman, J. N. & Strano, M. S. Electronics and optoelectronics of two-dimensional transition metal dichalcogenides. Nat. Nanotechnol. 2012, 7, 699-712

8. Radisavljevic, B., Radenovic, A., Brivio, J., Giacometti, V. & Kis, A. Single-layer MoS2 transistors. Nat. Nanotechnol. 6, 147-150 (2015).

9. Yan E.X., Caban-Acevedo, M., Papadantonakis, K.M., Brunschwig, B.S., Lewis, N.S. Reductant-Activated, high-coverage, covalent functionalization of 1T-MoS2. ACS Materials Lett. 2, 133-139 (2020).

10. E. Garcia-Berrios, J. C. Theriot, M. D. Woodka and N. S. Lewis. Detection of ammonia, 2,4,6-trinitrotoluene, and common organic vapors using thin-film carbon black-metalloporphyrin composite chemiresistors. *Sensors and Actuators B Chemical*, **2013** , *188*, 761-767

11. Garcia-Berrios, T. Gao, D. Walker, B. S. Brunschwig and N. S. Lewis. Composites of carboxylate-capped TiO_2 nanoparticles and carbon black as chemiresistive vapor sensors. *Sensors and Actuators B-Chemical*, **2011** , *158*, 17-22

12. Hybrid Materials: Synthesis, Characterization, and Applications. Edited by Guido Kickelbick (Technische Universität Wien, Austria). Wiley-VCH Verlag GmbH & Co. KGaA: Weinheim. 2007. xviii + 498. ISBN 978-3-527-31299-3

Chapter 3

THE IMPORTANCE OF GOOD ELECTRICAL CONTACT AND STABILITY

Introduction

The ability to monitor the various components of air in various settings can be conducted through various analytical instruments. These vapor detectors hold tremendous potential in their applications for disease diagnostics, explosive (TNT) detectors for the aversion of potential harm, harmful chemical detectors in lab settings and etc.[1,2] However, to detect these compounds require highly sensitive and expensive instruments. In today's modern word, advanced technologies do exist that can detect and analyze minute quantities of vapor (parts per billion (ppb)) such as the gas chromatography (GC). However, these types of instruments are costly, requiring a trained technician to operate and to maintain. Such instruments are also bulky and heavy that hampers its mobility and practicality to various settings such as Africa.[1,4, 5] Even here in the United States, rising health care costs prevent many from seeking medical attention. An apparatus that is simple, portable and have low cost/power is needed.

Traditional chemical sensors use a strict "lock-and key approach", but limited knowledge of specific biomarkers as well as variability across individuals (diet, habits, etc), makes this a poor approach for biomarker detection in human breath. Work done by the Lewis Group at Caltech on the electronic nose, utilizes a collective array of sensors to produce a distinct pattern which is than translated into developing a "fingerprint" for its classification of an analyte. Each sensor is designed to be broadly cross-responsive, and not

reactive toward a specific individual analyte.[1,2,4,5] The group has previously explored various polymeric sensor films mixed with carbon black whereupon exposure to volatile organic vapors (VOCs) results in the analyte being adsorbed onto the film, altering the electrical conductivity (resistance) through changes in physiological properties of the films such as swelling and constricting.[1] By measuring the resistance change as various vapors are introduced, the device is kept relatively simple, easy to use and cheap. However, there are limitations to volumetric signal transduction because analytes with high vapor pressure will generate small signals because the equilibrium driving force favors keeping the analyte in the gas phase rather than in the solid phase.[1,3]

$$K = \frac{\rho RT}{\gamma MP^{\circ}}$$

Equation 1. Volumetric Signal transduction equation. K=Partition coefficient, ρ=sensor material density, T= sensor temperature, γ=activity coefficient of analyte within sensor material, M=Molar mass of the analyte, P°=vapor pressure of gaseous analyte of interest.

Due to the limitations stated earlier from volumetric signal transduction, focus was sought toward an amplification scheme. Specifically, by utilizing the concepts of the silver-mirror reaction (Tollen's reagent), this project sought to use gold-nanoparticles capped with a monolayer of ligands equipped with terminal amines (instead of using a liquid ammonia solution) along with $AgNO_3$ (NaOH can be added: Tollen's reagent can be created with just ammonia and silver nitrate) to create silver nanoparticles within the film when it comes into contact with aldehydes (equation 2).[7,9] Tollen's reagent is a chemical reagent that is used to conduct chemical tests to detect aldehydes. The reagent is typically made with AgNO3,

ammonia groups, and NaOH as shown in equation 2, however NaOH is not necessary because as long as sufficient amine groups are present, diamminesilver(I) complex, $[Ag(NH_3)_2]^+$ can still be formed (will at first form silver oxide, but as amine groups are added, the complex will form).[9,11] A "positive" indication results in the silver complex reacting with the aldehyde to form a carboxylic acid and precipitate elemental silver. In the presence of a small amount of aldehyde, silver nanoparticles are formed as shown in equation 3. The reagent also can be used to test for terminal alkynes, where a yellow precipitate (acetylide) will form.[4a,b]

Equation 2. Preparation of Tollen's reagent, a colorless, basic aqueous solution that coordinates with ammonia to create $[Ag(NH_3)_2]NO_3$ or $[Ag(NH_3)_2]^+$.

$$2\ AgNO_3 + 2\ NaOH \rightarrow Ag_2O + 2\ NaNO_3 + \ H_2O$$

$$2\ AgNO_3 + 4\ NH_3 + 2\ NaNO_3 + H_2O \rightarrow 2[Ag(NH_3)_2]NO_3 + 2\ NaOH$$

Equation 3. Tollen's reagent reacts with the aldehyde to form a carboxylic acid and precipitates elemental silver.

$$[Ag(NH_3)_2]^+ + RCHO + H_2O \rightarrow 2\ Ag_{(s)} + 4\ NH_3 + RCO_2H + 2\ H^+$$

By utilizing gold nanoparticles capped with ligands equipped with terminal amines along with NaOH and $AgNO_3$, a sensitive amplification scheme can be created. In a film of the functionalized gold nanoparticles and $AgNO_3$ (with or without NaOH), the $AgNO_3$ will cross react with the terminal amine ends of the gold nanoparticles to form the necessary $[Ag(NH_3)_2]^+$.[4a,b,c] And as small amounts of gaseous aldehydes are introduced to the film, the $[Ag(NH_3)_2]^+$ will react with the gaseous aldehyde to form silver nanoparticles and also start to coat the gold nanoparticles with silver to create Au/Ag nanostructure, decreasing the

resistance. A possible resistance change is also expected when the Tollen's reagent nanoparticle film comes into contact with terminal alkyne groups due to formation of acetylide, a yellow precipitate. Agarose gel was selected to hold the tollen's reagent and gold nanoparticles because of its porosity, ease of use and durability.

Methods

Preparation of amine terminated Au nanoparticles through deprotection

Briefly, citrate (10mM) was added injected into an aqueous solution of a 100ml $HAuCl_4$ (1mM). Solution should change color from pale yellow to wine red. Finally, the solution as cooled to room temperature under stirring and store at 4C for further use.

Preparation of amine terminated Au nanoparticles through deprotection

Briefly, 10ml of NaBH4 (10mM)was added slowly drop-wise into a mixture of di-boc-cystamine (38.8 mM) ,100ml $HAuCl_4$ (1mM) and TOAB (10mM). Solution should change color from pale yellow to wine red. Finally, the solution as cooled to room temperature under stirring and store at 4C for further use. To deprotect and expose the amine terminal group, 10ml solution (5mM) of trifluoracetic acid was added slowly and stirred for 30min. Trifluoracetic acid was removed through vacuum rotary evaporator.

Tollen's stock solution Preparation

1ml $AgNO_3$ solution (0.5M) was added to 1040ul aqueous ammonia (25%-28%), followed by addition of NaOH (3M, 650ul). Water was used to reach the final volume of 20mL. This tollens stock contains about 25mM of $[Ag(NH_3)_2]OH$ and 1 mM free NH_3 H_2O.

Preparation of agarose gels

To boiled water (5mL) agar powder was added (varying concentrations-started at 0.1g). The solution was heated and stirred until the agar powder dissolved completely. Agar solution (1.5 mL) was pipetted to a Petri dish (3.5cm). When the agar solution was cooled to about 50C, Au NPs colloidal (6nM, 0.4 mL) and Tollens reagent (0.5 mL0 were added into the agar solution. Finally, the agar solution was molded into gel by placing the Petri dish into a refrigerator at 0C for 2min. The as-prepared agarose gel was cut into smaller ones with spherical shape for further use.

Agarose gel, colorimetric detection of HCHO

The agarose gel was immersed into 5mL of HCHO aqueous solution with various concentration. 30min later they were taken out and photographed, carried out at ambient temperature (28C)

Results

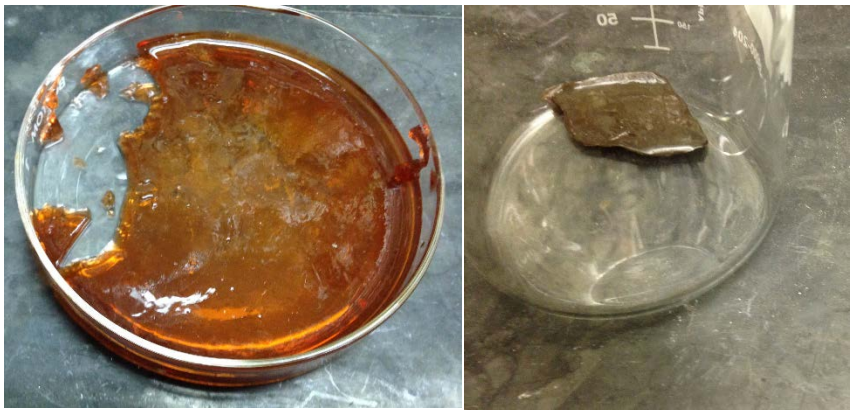

Figure 1. Initial colorimetric detection of agarose gel mixed with citrate-NP. The picture on the left shows citrate Au nanoparticles and Tollen's reagent loaded agarose gel that was molded and cooled, and pieces of the agarose gel were placed in dilute concentrations of acetaldehyde. The picture on the right: Agarose gel that changed color when placed in 10% acetaldehyde solution and water.

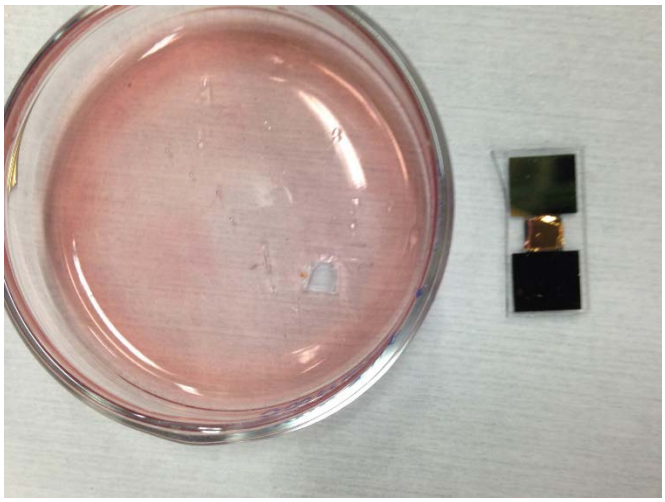

Figure 2. Molded agarose gel mixed with citrate-NP, and Tollen's reagent. After molding and cooling, pieces of the gel were placed on interdigitated electrodes.

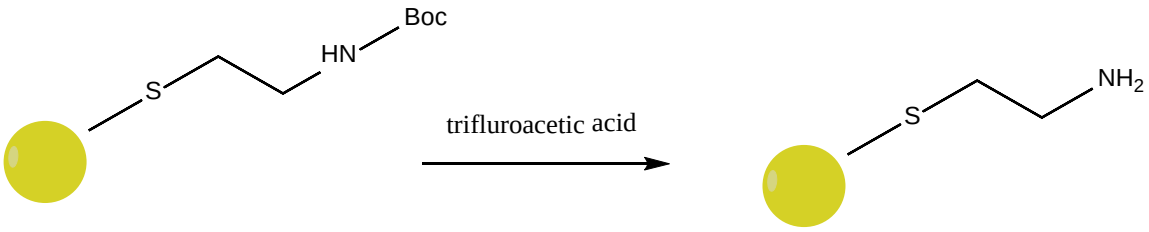

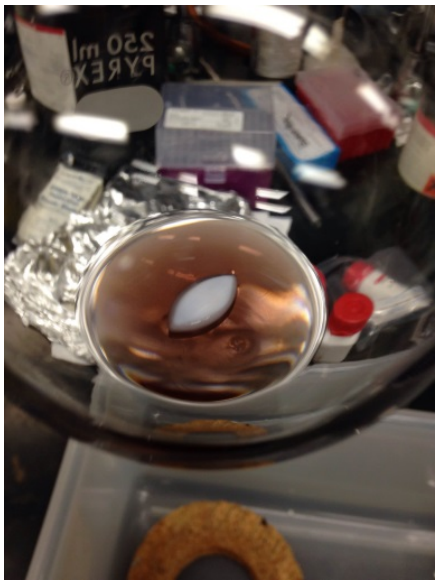

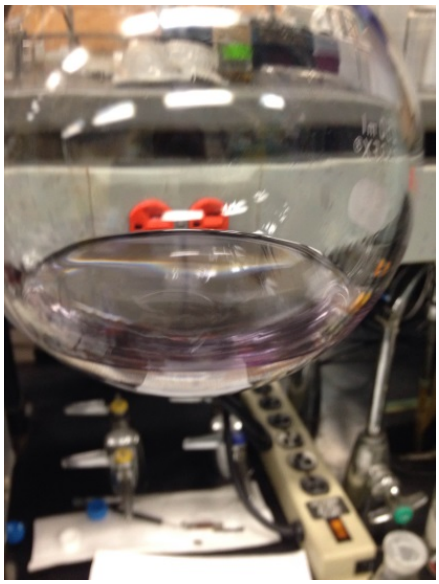

Figure 3. Synthesis of amine terminated Au nanoparticles by using di-boc-cystamine as the initial protecting group and deprotecting it through usage of trifluoracetic acid.

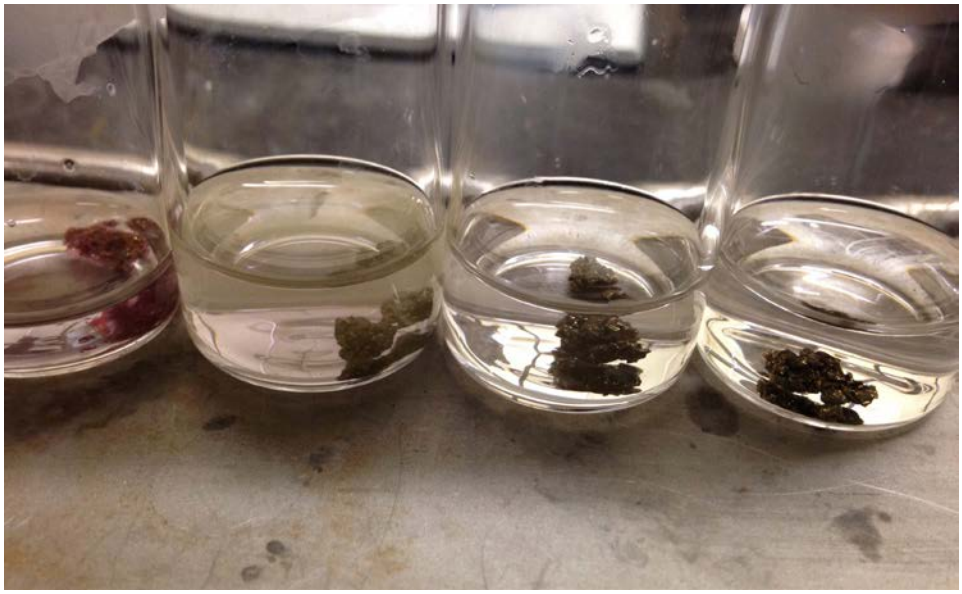

Figure 4. Hydrogels were used to "load" Tollen's reagent into the polymer. The left most exhibited a light purple color after Tollen's reagent absorption and darkened in color due to silver nanoparticle formation in varying concentrations of acetaldehyde in water (right 3).

Discussion/results

Initial testing was conducted by creating agarose gel loaded with Tollen's reagent and citrate capped gold nanoparticles. The loaded agarose gel was placed in dilute aqueous concentrations of acetaldehyde to conduct preliminary tests to ensure the sensor will react with acetaldehyde. The dilutions were conducted at 50%, 25%, and 10% using water. All gels placed in the 50%, 25% and 10% solutions exhibited a color change; figure 1 shows a dark color change in 10% solution. The color change was expected because due to the silver complex forming silver particles after reacting with the acetylaldehyde.[7,8,13] After this preliminary testing, a 1.3% agarose gel loaded with Tollen's reagent and citrate capped gold nanoparticles was cut and placed onto an interdigitated electrode as shown in figure 2. Optimized standardization on percent agarose usage was conducted where it was found that going below 0.7% agarose gel, the material fell apart, while going above 3% viscosity made the gel too stiff so that it did not adhere to the electrode well.

Varied percent agarose gel was tested and placed on the electrode with a baseline resistance ranging from 50k-200k ohms. However, upon exposure, signals were very hard to obtain as shown in SI 1. Poor signal was possibly due to poor adherence of the agarose gel and the unstable nature of tollen's reagent (silver amine complex). Therefore, two different approaches were used. The 1st approach was to provide stability to the silver amine complex; utilizing amine terminated Au nanoparticles as shown in figure 3, where the end group of the amine terminated Au nanoparticles could provide stability through its nitrogen end group. The 2nd method involved exploration of different holding mediums beside agarose gel such as hydrogels as shown in figure 4.[6,10,11] However, the amine terminated Au

nanoparticles were shown to be extremely unstable and crashed out within 10min of deprotection as shown in SI 2. For the 2nd method, the hydrogels absorbed Tollen's reagent well, however it had poor adherence to the interdigitated electrode and as soon as the hydrogel dried, the hydrogel darkened in color, and the silver amine complex crashed out.

Conclusion

Through this it was found that good contact and stability within the material is essential to achieve good signal, where without a stable baseline resistance, a sensor for the electronic nose cannot be produced.

References

1. Gao, T., Woodka, M.D., Brunschwig, B.S., Lewis, N.S. Chemiresistors for Array-Based Vapor Sensing Using Composites of Carbon Black with Low Volatility Organic Molecules. *Chem. Mater*. **2006**, 18, 5193-5202

2. E. Garcia-Berrios, J. C. Theriot, M. D. Woodka and N. S. Lewis. Detection of ammonia, 2,4,6-trinitrotoluene, and common organic vapors using thin-film carbon black-metalloporphyrin composite chemiresistors . *Sensors and Actuators B-Chemical*, **2013** , *188*, 761-767

3. Garcia-Berrios, T. Gao, D. Walker, B. S. Brunschwig and N. S. Lewis. Composites of carboxylate-capped TiO2 nanoparticles and carbon black as chemiresistive vapor sensors *Sensors and Actuators B-Chemical*, **2011** , *158*, 17-22

4. Garcia-Berrios, T. Gao, J. C. Theriot, M. D. Woodka, B. S. Brunschwig and N. S. Lewis. Response and Discrimination Performance of Arrays of Organothiol-Capped Au

Nanoparticle Chemiresistive Vapor Sensors. *Journal of Physical Chemistry C*, **2011** , *115*, 6208-6217

5. Garcia-Berrios, T. Gao, M. D. Woodka, S. Maldonado, B. S. Brunschwig, M. W. Ellsworth and N. S. Lewis. Response versus Chain Length of Alkanethiol-Capped Au Nanoparticle Chemiresistive Chemical Vapor Sensors. *Journal of Physical Chemistry C*, **2010**, *114*, 21914-21920

6. Zeng, J., Fan, S., Zhao, C., Wang, Q., Zhou, T., Chen, X., Yan, Z., Li, Y., Xing, W., Wang, X. A colorimetric agarose gel for formaldehyde measurement based on nanotechnology involving Tollens reaction. Chem. Commun., **2014**, 50, 8121.

7. Fink, J., Kiely, C.J., Bethell, D., Schiffrin, D.J. Self-Organization of Nanosized Gold Particles. Chem. Mater. **1998**, 10, 922-926

8. Reaction of Amines.

https://www2.chemistry.msu.edu/faculty/reusch/virttxtjml/amine2.html

9. Gibbs. H.D. Phenol Tests. 1. A Classification of the Tests and a Review of the Literature. Chem. Re., **1936**, 3, 291

10. Sun, J., Zhao, X., Illeperuma, W.R.K., Chaudhuri, O., Oh, K.H., Mooney, D.J., Vlassak, J.J., Suo, Z. Highly stretchable and tough hydrogels. *Nature*. **2012**, 489, 133-136.

11. Buenger, D., Touz, F., Groll, J. Hydrogels in sensing applications. *Prog. Polym. Sci.* **2012**, 37, 1678-1719

12. Porter, T.L., Stewart, R., Reed, J., Morton, K. Models of Hydrogel Swelling with Applications to Hydration Sensing. *Sensors*. **2007**, 7, 1980-1991

13.Takuro Niidome, T., Nakashima, K., Takahashi, H., Niidome, Y. Preparation of primary amine-modified gold nanoparticles and their transfection ability into cultivated cells. Chem.

Commun., **2004**, 197

Supporting Information

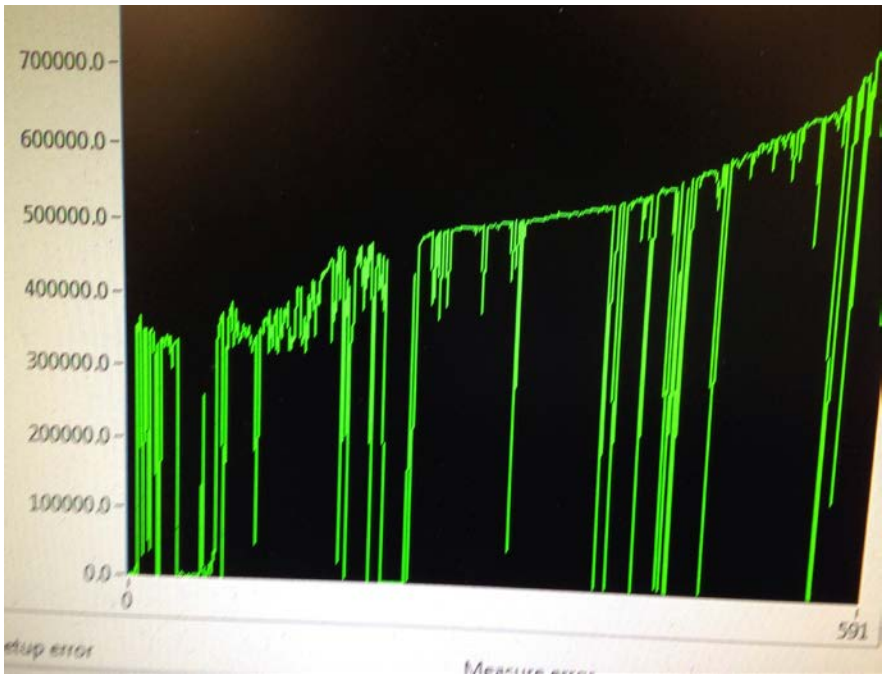

SI 1. Example baseline/experiment run of 1.3% agarose gel loaded with citrate Au nanoparticles and Tollen's reagent. The baseline signal was non-existent and unstable.

SI 2. Amine terminated nanoparticles were unstable and crashed out soon after boc-deprotection after addition of trifluoracetic acid.